Chapter 2

Detector for the Linear Collider

General Detector Concepts and Detector Performance
Conveners: M. Martinez, D.J. Miller, M. Piccolo

Working Group: A. Andreazza, M. Battaglia, G. Blair, G. Daskalakis, A. Juste, A. Kyriakis, C. Markou, H.U. Martyn, H. Nowak, I. Riu, M. Sachwitz, H.J. Schreiber, D. Schulte, R. Settles, R. Shanidze, C. Shepherd-Themistocleous, S. Shichanin, E. Simopoulou, R. Vuopionperä, C. Troncon

Detector Subsystems
Conveners: M. Mazzucato, D. Saxon, R. Settles

Working Group: S. Aïd, A. Andreazza, P. Bambade, T. Barklow, W. Bartel, M. Battaglia, R. Bellanzzini, S. Bertolucci, G. Blair, R. Brinkmann, I. Brock, R. Brown, J. Bürger, P.J. Bussey, M. Caccia, P. Checchia, G. Coignet, P. Colas, P. Clarke, C. Damerell, M. David, A. De Roeck, E. Elsen, E. Fernandez, Y. Giomataris, T. Greenshaw, R. Heuer, C. Heusch, N. Holtkamp, P. Hüntemeyer, P. Janot, L. Jönsson, F.P. Juster, B.J. King, F. Kircher, V. Korbel, U. Kötz, Y. Kurihara, P. Le Du, M. Leenen, W. Lohmann, C. Luci, L. Mandelli, M. Martinez, C. Meroni, J. Meyer, D. Miller, R. Nahnhauer, O. Napoly, R. Nania, R. Orava, M. Piccolo, M. Pohl, D. Reed, F. Richard, A. Rousarie, H.-G. Sander, U. Schneekloth, H.J. Schreiber, S. Schreiber, D. Schulte, C. Shepherd-Themistocleous, F. Simonetto, K. Sinram, A. Skillman, A. Sopczak, P. Steffen, H. Steiner, J. Steuerer, G. Tonelli, M. Tonutti, C. Troncon, C. VanderVelde, G. Vegni, A. Wagner, N. Walker, M. Weber, W. Wiedenmann, G.W. Wilson, K. Zapfe-Düren

Collider-Experiment Interface
Conveners: N. Holtkamp, M. Leenen, O. Napoly

Working Group: G. Bardin, R. Brinkmann, C. Cavata, S. Drozhdin, J.-P. Jorda, N. Mokhov, M. Sachwitz, H.J. Schreiber, S. Schreiber, D. Schulte, R. Settles, K. Sinram, N. Walker, K. Zapfe-Düren

Contents

2.4 Interface between Collider and Experiment

This section is devoted to the accelerator components or beam related aspects which either influence the design of the detector or are imposed by the detector performance. The machine and beam parameters are taken from the TESLA design, with SBLC parameters given in parentheses.

2.4.1 Beam Delivery System

The beam delivery system shown in Fig. 2.4.1 is the transfer line which transports the beam from the linac exit to the interaction point (IP) of the collider. The linac position with respect to the tunnel is shown in Sections 3.10 and 4.10 for TESLA and SBLC. The main function of the beam delivery system is to demagnify the beams and to bring them to collisions with spot sizes of $845\,\mathrm{nm}\times 19\,\mathrm{nm}$ ($335\,\mathrm{nm}\times 16\,\mathrm{nm}$) at the center of the detector. The overall demagnification from linac to IP is mostly produced by a strongly focusing quadrupole doublet 3 m (2 m) distant from the IP, integrated in a 140 m (125 m) long telescopic final transformer.

Even with the small, around $30\,\mu$rad, angular divergence of the beam at the IP, the chromaticity of this last doublet, roughly given by the ratio $\hat{\sigma}_Q/\sigma^*$ of the maximum beam size in the last doublet to the beam size at the IP, is too large in comparison with the expected relative energy spread of 10^{-3} ($3.5{\cdot}10^{-3}$) of the incoming beam. The final transformer is therefore preceded by a 330 m (380 m) long S-shaped Chromatic Correction Section (CCS) where sextupoles, located in dispersive regions, create the necessary quadrupole correction for the off-energy particles. The energy bandwidth of this correction determines the energy acceptance of the whole system.

The transverse beam tails passing through the doublet quadrupoles produce synchrotron radiation which in turn can be a source of background in the detector. The photon energies and angles are maximum in the last doublet where masking is difficult. The beam halo and the low energy tail, possibly generated in the linac, are therefore scraped off in the collimation section by collimators placed at maxima of the horizontal and vertical betatron and dispersion functions. The 390 m (610 m) long collimation section, also S-shaped, is located upstream from the CCS and separated from it by about 210 m (330 m) of straight beam instrumentation and tuning sections.

This beam delivery system has been designed to allow for an adiabatic upgrade of the collider beam energy from 250 to 400 GeV for TESLA (250 to 500 GeV for SBLC) by simply increasing the magnet strengths without changing the geometry of the beam line nor the magnets.

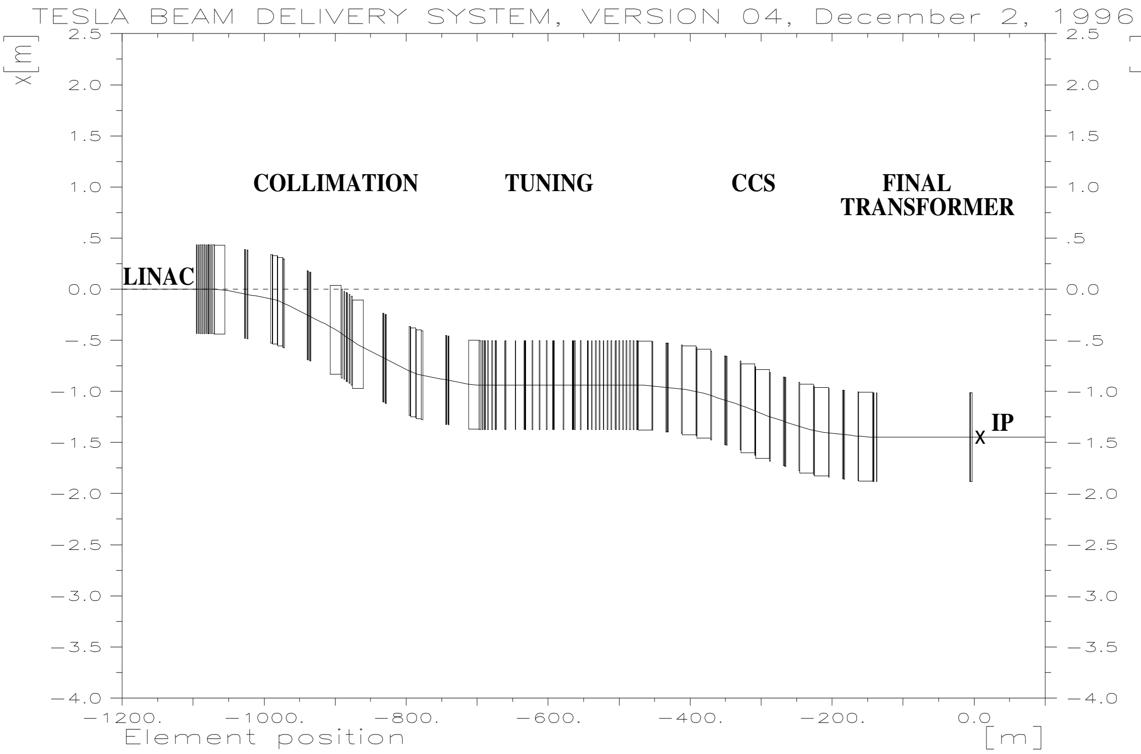

Figure 2.4.1: *Magnet layout and horizontal view of the TESLA beam delivery system from the Linac exit ($s = 0$ m) to the interaction point ($s = 1100$ m). The boxes indicate the position of the magnets.*

2.4.2 Interaction Region Layout

The interaction region layout is shown in Fig. 2.4.2 for TESLA. Since the doublet quadrupoles and cryostat are inside of the detector, the 3 T detector solenoid field is superimposed over the quadrupole field which precludes the use of an iron yoke to contain the quadrupole stray fields. For a quadrupole gradient of 250 T/m, the magnetic field reaches 8.4 T at its maximum on the conductor, and is only $5{\cdot}10^{-3}$ T at 600 mm radius [1]. The inner radius of the beam pipe inside the quadrupole is 24 mm, the outer radius of the cryostat 148 mm. The two 4.25 m long cryostats, facing each other on both sides of the IP, are separated by 5.5 m, the quadrupoles by 6 m.

The quadrupoles are covered by tungsten masks to suppress background from particles hitting the quadrupoles. Inside the masks the beam pipe reaches its smallest inner radius of 18 mm, while the radius is 40 mm at the tip of the mask (see Fig. 2.4.10). At the position of the vertex detector the radius is decreased to 20 mm – a more detailed

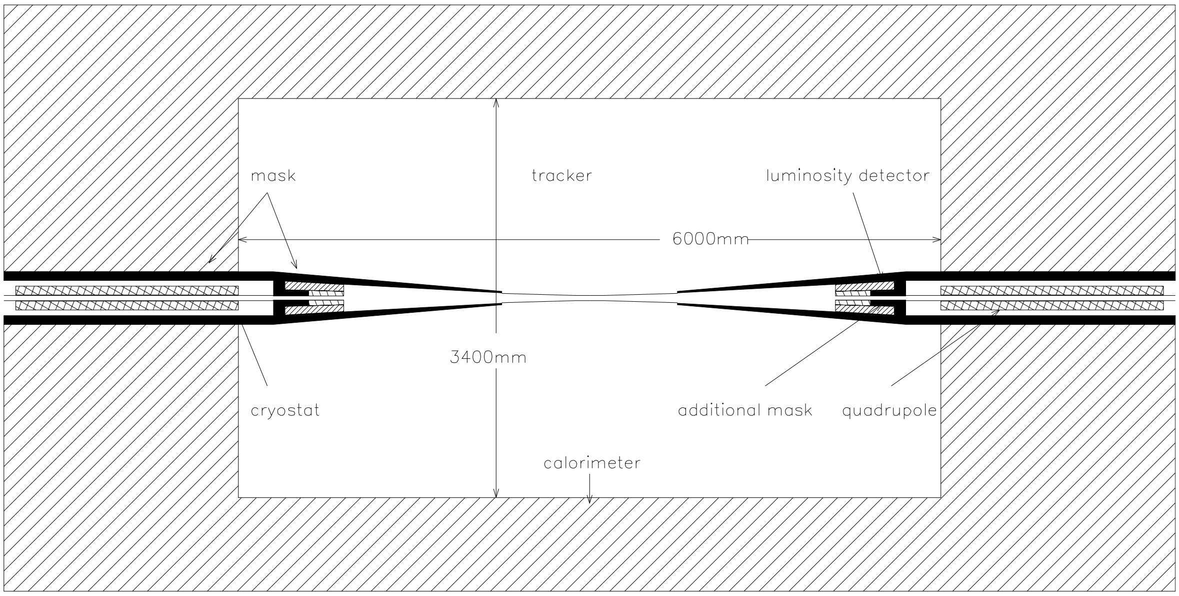

Figure 2.4.2: *TESLA (500 GeV c.m.) interaction region layout. The inner region is reserved for tracking. The hatched area represents the calorimetry (outer dimensions are arbitrary).*

description is given in section 2.4.4.

2.4.3 Accelerator Backgrounds

2.4.3.1 Synchrotron Radiation

Synchrotron radiation photons emitted by the incoming beam in the magnetic field of the last doublet quadrupoles has been identified as a major source of detector background at the SLC [2]. Although the average emitted power is only 35 W for TESLA (37 W for the SBLC), the average photon critical energy of 3.6 MeV (4.3 MeV) in the last quadrupole, is above the pair creation threshold. These photons are therefore difficult to shield and particularly harmful if they hit the inner part of the detector.

As can be seen from Fig. 2.4.3 the stay clear condition for the diverging photon flux is more constraining than the stay clear of the incoming beam itself. Requiring that all synchrotron radiation photons clear the exit aperture of the opposing doublet and the exit face of the detector implies that the incoming beam transverse tails do not extend beyond $14\,\sigma_x \times 46\,\sigma_y$ ($7\,\sigma_x \times 18\,\sigma_y$). For a circular aperture of TESLA, the collimation requirement for rectangular collimator apertures $n_x \times n_y$ in unit beam

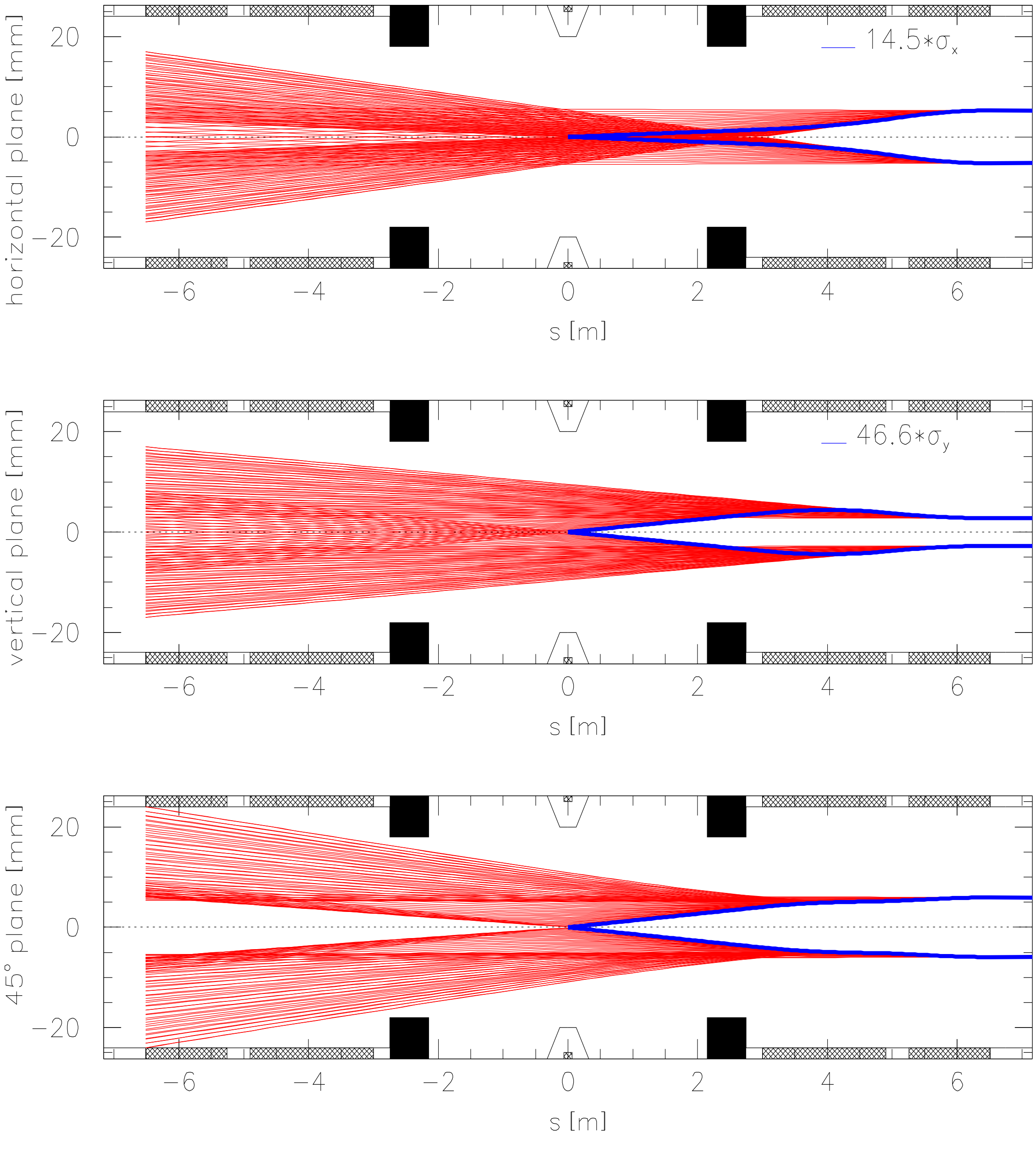

Figure 2.4.3: *Envelopes of synchrotron radiation photons emitted along the TESLA (500 GeV c.m.) last doublet quadrupoles through the vertex detector and opposing doublet apertures. Thick lines represent the envelopes of the incoming beam (entering from the right).*

sigmas, is actually given by

$$(n_x/14)^2 + (n_y/46)^2 = 2$$

in such a way that the photon flux fills a rectangle inscribed in the beam pipe aperture circle. Compared to the SLC beam collimation of $5\,\sigma_x \times 9\,\sigma_y$, these collimation requirements are quite loose. In fact, for the beam population considered, only non-gaussian tails can populate the beam at such numbers of sigmas. Generation of such tails in the linac is difficult to model. Therefore the proportion of beam intercepted by the collimators is difficult to predict, as is the background from muons produced at the collimator discussed in the following section.

Other sources of synchrotron radiation include the upstream quadrupoles of the final telescope and the last bending magnet of the CCS. The collimation requirements concerning the upstream quadrupoles are about 3 times looser than for the final doublet. In the case of TESLA, the photon flux originating from the last CCS dipole has a critical energy of 1.3 MeV. It must be horizontally collimated to fit through the detector inner beam pipe aperture. To achieve this, it is intended to use the beamstrahlung main collimator with 4 mm aperture radius located half-way of the final telescope, as shown in Fig. 2.4.5.

In conclusion, the collimation system can be designed such that no synchrotron radiation photon hits, directly or indirectly, any part of the detector.

2.4.3.2 Muons

In e^+e^- linear colliders muons produced in electro-magnetic beam-nucleon interactions in the beam delivery system can contribute an intolerable background in the detector. When electrons or positrons strike beam-line elements, e.g. the beam-halo collimators, muons are produced by a variety of mechanisms:

- Bethe-Heitler process with $\gamma \mathrm{Z} \rightarrow \mu^+\mu^-\mathrm{Z}$
- photo-production of pions $\gamma \mathrm{Z} \rightarrow \pi(\rightarrow \mu\nu) + \text{anything}$
- direct e^+e^- annihilation, $e^+e^- \rightarrow \mu^+\mu^-$.

Of these, the most important muon source is the Bethe-Heitler process which produces about an order of magnitude more muons than the other processes.

The estimation of the muon background expected in the detector takes into account the beam-line elements of the TESLA and SBLC beam delivery systems (see section 2.4.1), the transverse dimensions of the corresponding tunnels and the positions of the beams as indicated in Fig. 2.4.1. Two independent programs were used, one developed at SLAC [3] and adapted for this study, and the other based on the CERN package GEANT [4][5], so that some confidence on the reliability and an idea

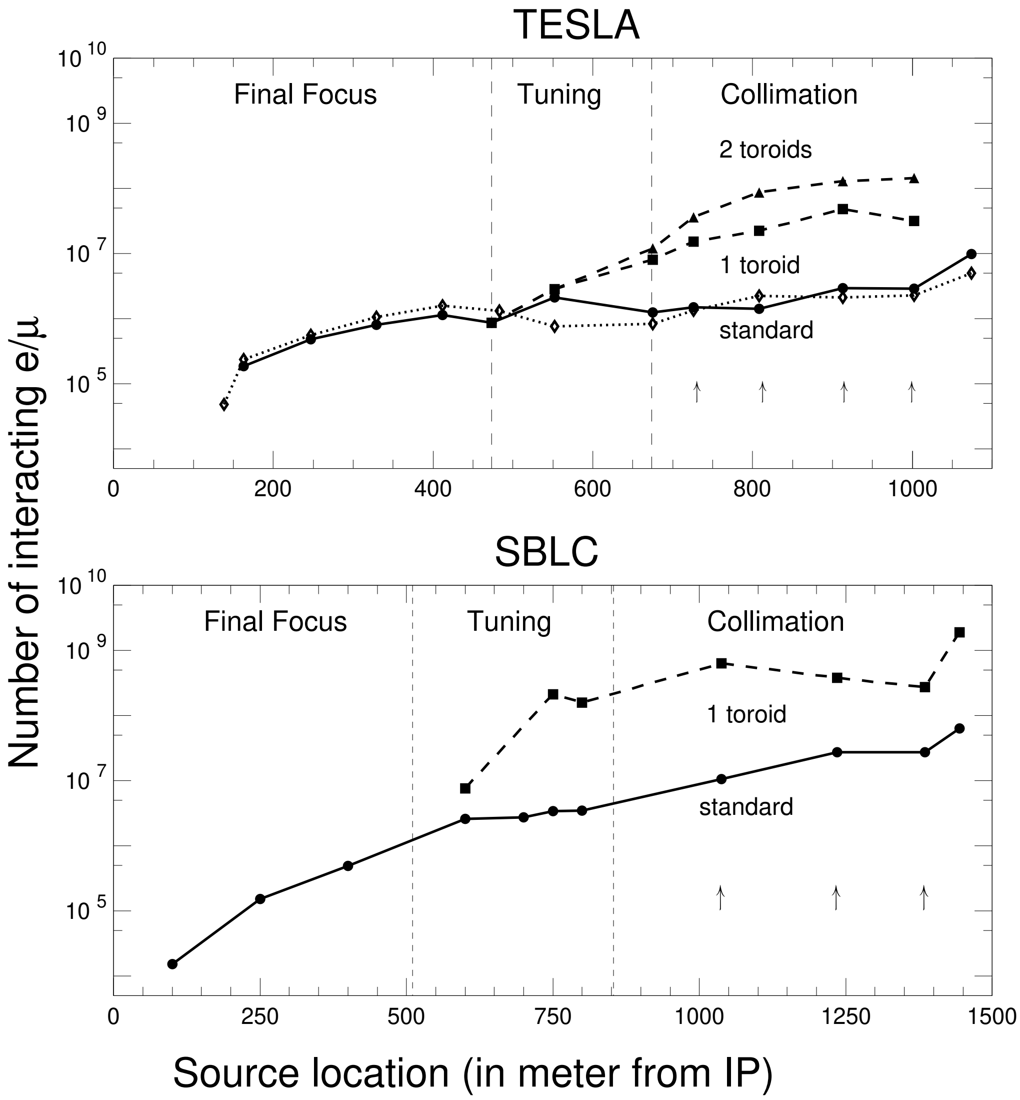

Figure 2.4.4: *The number of beam particles required to hit the source in order to produce one muon in the detector as a function of the source location for TESLA and SBLC (*500 GeV *c.m.). The arrows indicate the locations of the collimators, the dotted line is calculated using the GEANT based program developed for this study [5], the other lines are calculated using a program developed at SLAC [3].*

of the systematic errors have been obtained. The detector is approximated by a disk of 5 m radius, centered at the interaction point. All muons which hit the detector are counted, irrespective of their energy. The source of the muons has been placed anywhere between the beginning of the collimation part and the IP. The muons have been produced randomly according to theoretical momentum and angular distributions [6] and tracked through the beam delivery system taking into account multiple coulomb scattering, energy loss, decay and bending in the magnetic fields, until they stop or reach the detector.

Figure 2.4.4 shows for the TESLA and SBLC designs the number of beam particles $N_{\rm int}$ which have to interact in order to produce one muon in the detector, as a function of the muon source location. Interactions of beam particles are likely to happen in the beam-halo collimators (spoilers) which are located several hundreds of meters upstream of the IP. Muon fluxes resulting from these positions are indicated by arrows in Fig. 2.4.4. Averaging over the spoiler positions yields $N_{\rm int} = 2 \cdot 10^6$ for TESLA and $N_{\rm int} = 2 \cdot 10^7$ for SBLC. The difference between TESLA and SBLC arises mainly from the different beam line positions in the tunnel and the material to be installed.

Beside this direct muon production, muons can also be produced by interactions of electro-magnetic shower particles (photons, electrons, positrons) created when the beam strikes a spoiler. These particles are to a great extent absorbed in the iron absorbers positioned further downstream. Their rates and energy distributions in the absorber have been calculated and, in turn, used as input of the muon production and tracking programs. The rate of such muons has been found to be very similar to that of the "directly produced" muons.

Finally, the allowed fractional beam loss on the spoilers $\epsilon_{\rm lost}$, in order to have less than one muon in the detector, is given by the ratio of tolerable number of intercepted beam particles $N_{\rm int}/2$, where the factor of 2 accounts for the electro-magnetic showers, to the total number of particles in the two beams $2N_{\rm e}N_{\rm b}$, where $N_{\rm e}$ is the number of particles per bunch and $N_{\rm b}$ is the number of bunches. For TESLA with its large bunch spacing no pile-up of muons is expected and $N_{\rm b} = 1$, while for the SBLC design, a detector read out time of 100 ns is assumed, thus $N_{\rm b} = 17$, in such a way that

$$\begin{aligned} \epsilon_{\rm lost} &= 1.4 \cdot 10^{-5} \qquad && \text{(TESLA)} \\ \epsilon_{\rm lost} &= 2.8 \cdot 10^{-5} \qquad && \text{(SBLC).} \end{aligned}$$

If, for some unexpected reasons, the muon rate will be intolerably large, additional devices like magnetized iron toroids [3] or nested magnetized iron cylinders with opposite-polarity azimuthal magnetic fields [7] positioned downstream of the muon source are able to reduce the muons considerably. An example of such muon rate reduction is also shown in Fig. 2.4.4: here, one or two iron toroids of 9 m length each have been installed in the final focus section relatively close to the IP. They add one to two orders of magnitude of protection.

2.4.3.3 Beam-Gas

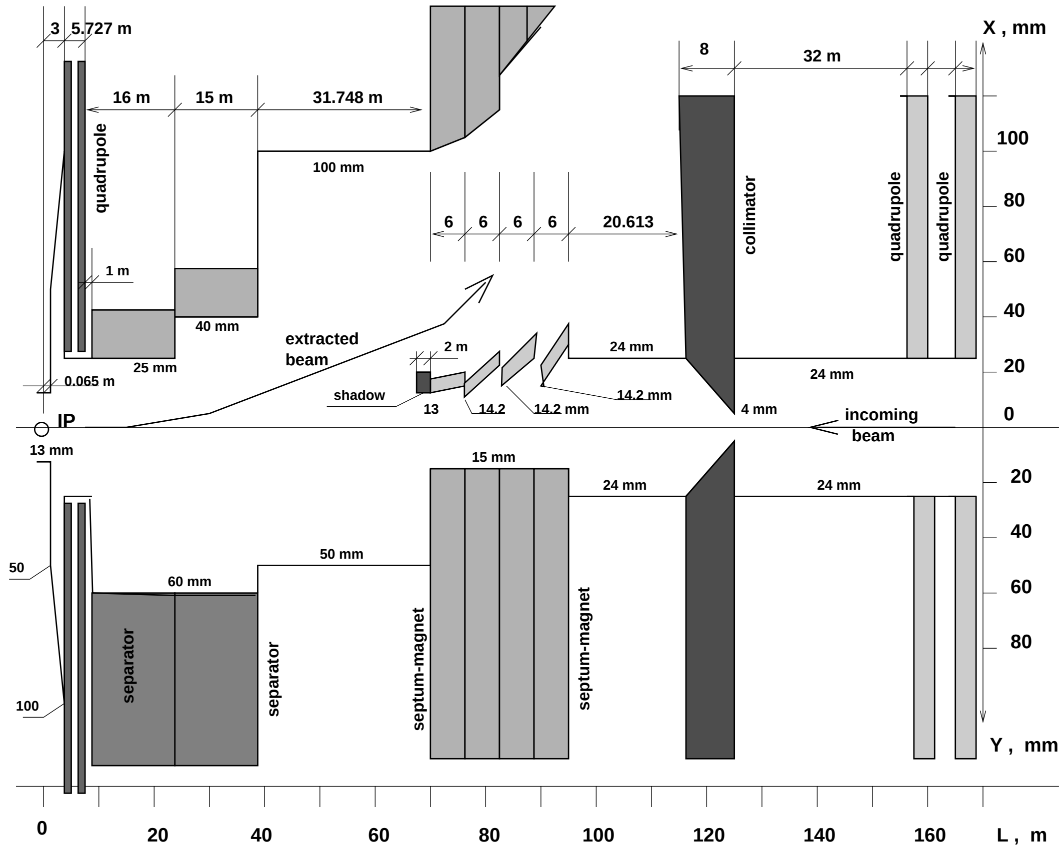

Figure 2.4.5: *TESLA (800 GeV c.m.) beam line aperture.*

The contribution to the background rates in the detector due to beam-gas interactions has been calculated using the same approach as [8, 9] for the TESLA 800 GeV design. Background rates for the 500 GeV design can be scaled down linearly with the energy. Interactions of the 400 GeV electron beam with residual gas, induced electro-magnetic showers, production of muons and hadrons and their transport are simulated with the latest version 13(96) of the MARS code [10]. Along with the detailed geometry and magnetic field description and advanced tracking algorithms for electro-magnetic and hadronic showers, the calculations include prompt muon production by electrons and photons (Bethe-Heitler pairs $\gamma Z \to Z\mu^+\mu^-$ and direct positron annihilation $e^+e^- \to \mu^+\mu^-$), muon production in π, K, charmed, and vector meson decays and the dimuon continuum, hadron production in photo-nuclear and deep inelastic muon interactions. The cut-off energies for particles in these calculations are 1 MeV for charged hadrons, muons and $e^\pm$, 0.2 MeV for photons and 0.5 eV for neutrons. The gas pressure is

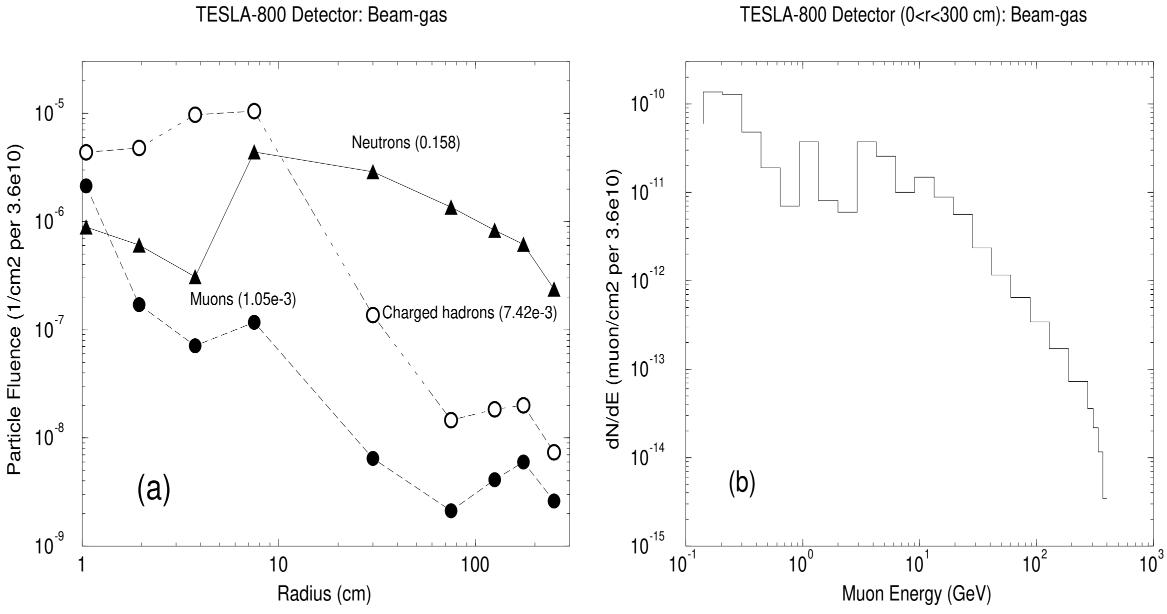

Figure 2.4.6: *TESLA (800 GeV c.m.) interaction region: (a) Muon, charged hadron, and neutron flux* ($1/\mathrm{cm}^2$) *per bunch due to beam-gas interactions in the final focus, as a function of the radius from the center of the detector. Indicated in the parenthesis are the integrated numbers of particles at the detector. (b) Radially averaged muon spectrum at the detector due to beam-gas interactions.*

assumed to be 10^{-7} mbar, and results can be linearly rescaled for other pressures. The geometry of the TESLA-800 beam line layout as it is used for the MARS simulations is shown in Fig. 2.4.5. Three-dimensional geometry and material descriptions of the final-focus quadrupoles, separators, septum magnets, shadow, collimator and drifts in the 170 m region from the IP are taken into account in the simulations. Magnetic fields in the final-focus quadrupoles (250 T/m) and septum magnet (0.08 and 0.12 T) are included as well. No detailed description of the detector, tunnel and experimental hall is included in the model at this stage.

Particle fluxes coming to the detector due to 400 GeV electron beam interactions with the residual gas in the 170 m long region in the IP vicinity are presented in Fig. 2.4.6(a) as a function of the distance from the beam axis. Charged hadrons dominate at small radii, but at $r \geq 10$ cm the main contribution is due to low-energy neutrons. Although the entire region is responsible for the production of background particles, soft neutrons are mostly produced in the few meter vicinity of the IP where details of the detector, tunnel and experimental hall geometry might affect the results. The energy spectrum of muons coming to the detector due to beam-gas interactions is shown in Fig. 2.4.6(b).

For the foreseen vacuum level of better than 10^{-8} mbar at the interaction region and 10^{-7} mbar in the beam delivery system, background from beam-gas interaction is negligible. The numbers given can be scaled linearly for different beam energies, bunch charges and vacuum pressure.

2.4.4 Beam-Beam related Backgrounds and Masking

The high charge density of the colliding beams produces strong electro-magnetic fields which bend the trajectories of the particles of the oncoming bunch. This focusing effect reduces the effective beam size and enhances the total luminosity. However, at these high energies, this beam-beam interaction also induces an intense emission of hard "beamstrahlung photons" which degrades the energy distribution of the beams during collision. The resulting dilution the luminosity spectrum is shown in Fig. 2.4.7 for the TESLA 500 GeV parameters. Keeping this dilution acceptable for the experiment sets a lower limit on the horizontal spot size, which in turn limits the luminosity.

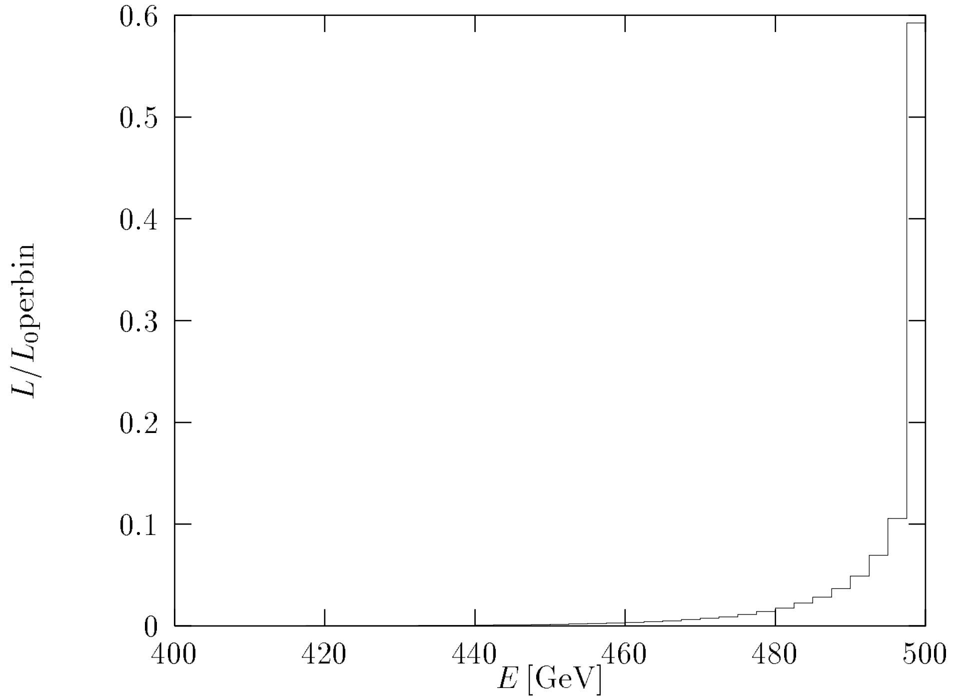

Figure 2.4.7: *Luminosity spectrum for TESLA (500 GeV c.m.) parameters, as resulting from beamstrahlung alone.*

The lowest part of the outgoing beam energy spectrum is plotted in Fig. 2.4.8 and their average energy loss δ, of the order of a few percent, is given in Table 2.4.1 for two sets of TESLA and SBLC parameters. As shown in Fig. 2.4.8, the outgoing beam energy spectrum is dominated by the bremsstrahlung spectrum, discussed later, for particle energies below 100 GeV. Tracking simulations show that, despite the emittance degradation, the outgoing beam particles originating from the IP lie within the acceptance of the opposing doublet as long as the particle energy is larger than 90 GeV.

One of the main background sources in the detector is the production of electron-positron pairs via coherent or incoherent processes in the beam-beam interaction. In

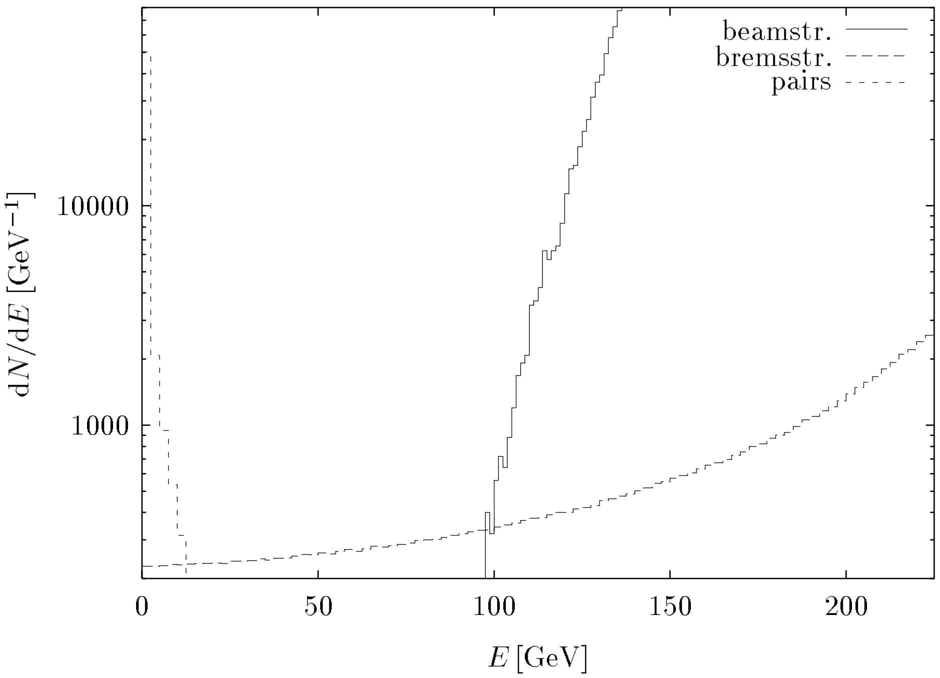

Figure 2.4.8: *The energy spectrum of the outgoing beam due to beamstrahlung effects and bremsstrahlung, and the spectrum of the particles due to pair production, for TESLA (*500 GeV *c.m.) parameters.*

addition beam particles can emit bremsstrahlung photons hard enough that the remaining low energy particle is lost inside the quadrupoles. Also relatively low energy hadronic events contribute to the background. The beamstrahlung is emitted into a very narrow cone of less than 0.5 mrad for the core and thus exits the detector safely without producing any direct background. It only enhances the production of pairs and hadrons due to beam-beam interaction.

In principle pairs can be produced via coherent and incoherent processes[3]. The coherent ones can be neglected if the beamstrahlung parameter Υ is smaller than

[3]The production of muon pairs is strongly suppressed compared to electrons due to their larger mass.

		TESLA		SBLC	
$E_{\rm cm}$	[GeV]	500	800	500	750
L	$[10^{33}\,{\rm cm}^{-2}{\rm s}^{-1}]$	6.0	5.7	5.3	5.5
δ	[%]	2.5	5.2	2.8	4.8
N_P	$[10^3]$	96	180	24	70
E_P	$[10^3\,{\rm GeV}]$	164	650	53	290
$N_\perp$		31	46.5	7.1	17
$N_{\rm Hadr}$		0.13	0.46	0.04	0.17
$N_{\rm MJ}$	$[10^{-2}]$	0.3	1.6	0.1	0.66

Table 2.4.1: *Luminosity L, average energy loss δ, and background for different TESLA and SBLC parameter sets. N_P pair particles with a total energy of E_P are produced per bunch crossing of which $N_\perp$ have transverse momentum in excess of* 20 MeV/c *and an angle with respect to the beam axis of more than* 150 mrad. *The number of hadronic events is $N_{\rm Hadr}$ including $N_{\rm MJ}$ minijet pairs with a transverse momentum of more than* 3.2 GeV/c.

0.3 [11], as is the case for TESLA and SBLC. Three main processes contribute to the incoherent production of electron-positron pairs ee $\to$ ee(e^+e^-), e$\gamma \to$ e(e^+e^-) and $\gamma\gamma \to e^+e^-$, where the real photons arise from beamstrahlung. The first two processes can be calculated using the equivalent photon approximation, in which the electrons (and positrons) are replaced by a spectrum of photons. Most of the particles are produced at a small angle but are strongly deflected by the fields of the beams. If the particles move initially in the direction of the beam with the same charge, they are over-focused, if they move into the opposite direction they are bent outwards. The maximal angle the particles can receive from the deflection is a function of their energy. Only a small number of particles is produced at a larger angle. The production and deflection of the pairs is simulated with the program Guinea-Pig [12].

The number of particles produced with the standard TESLA parameters (the first column in Table 2.4.1) is about 10^5 per bunch crossing with a total energy of $1.6 \cdot 10^5$ GeV. Figure 2.4.9 shows the angle and transverse momentum of the pair particles after the bunch crossing. The numbers for the other parameter sets are listed in Table 2.4.1.

Another process that produces low energy particles is bremsstrahlung. In this process a beam particle emits a hard photon in the field of a single particle of the other bunch. The photon escapes through the beam pipe, while the remnant beam particle contributes to the background. It is calculated using the equivalent photon approximation. The resulting spectrum of low energy beam particles is almost flat for small energies. These particles deposit a total energy of about $2{\cdot}10^5$ GeV per bunch

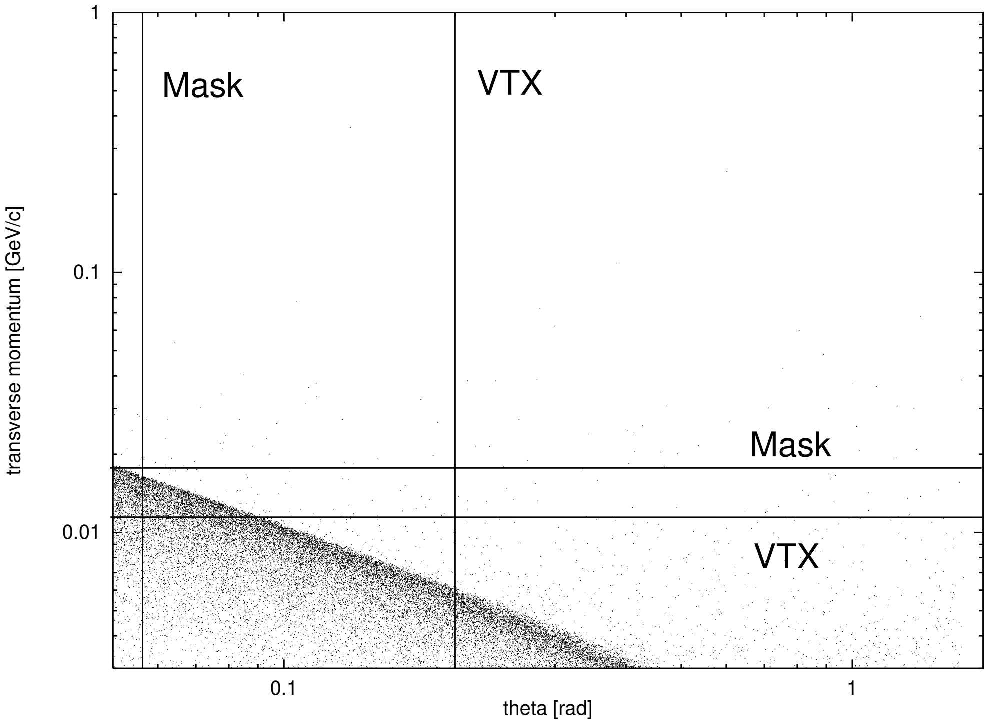

Figure 2.4.9: *Distribution after the interaction of the angle theta with respect to the beam axis and the transverse momentum of the particles from pair creation for TESLA (*500 GeV *c.m.) parameters. Indicated are the geometrical inner boundaries of the mask and the vertex chamber (VTX).*

crossing in the quadrupoles. The energy spectra of the pairs, and of the beam particles due to bremsstrahlung and beamstrahlung is shown in Fig. 2.4.8.

To estimate the background induced by the pairs and bremsstrahlung a detector simulation was performed on the basis of GEANT using the mask described below.

The large number of particles hitting the final quadrupoles leads to a high number of backscattered photons in the detector if it is not protected. The protection can be achieved with a conical mask mounted to a cylindrical one, as shown in Fig. 2.4.10. If the cone was extended its tip would be at the interaction point. The inner opening angle of the mask of 55 mrad is determined by the space requirement of the cryostat, which has a radius of 148 mm and starts at $|z| = 2750$ mm. The mask starts at $|z| = 750$ mm with an inner radius of $r_i = 41.7$ mm to let pass all the particles below the edge in Fig. 2.4.9 safely. The outer opening angle of 83 mrad is chosen to achieve the required thickness of the cylindrical part.

To minimize the thickness of the mask it is made of tungsten. In the electro-

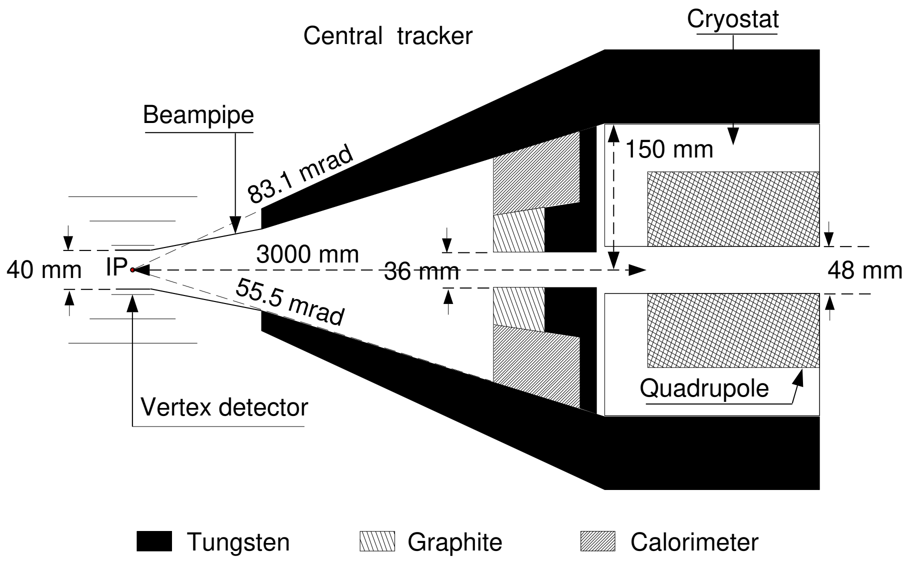

Figure 2.4.10: *Possible mask layout to suppress the background from pair creation for TESLA (*500 GeV *c.m.).*

magnetic showers a large number of photons is produced that are scattered out of the quadrupoles. While the spectrum of these photons peaks at a few hundred keV the most dangerous are those with energies of a few MeV since their total cross section in matter is small. The total energy of all photons outside the mask at a position $|z| < 5\,\mathrm{m}$ is about 400, 55, 10 or 2 GeV for mask thicknesses of 25, 50, 75 or 100 mm, respectively. A thickness of 75 mm was chosen to have a photon energy of less than 10 GeV outside the mask. For this thickness, about 600 photons per bunch crossing have to be expected in the drift chamber. This number depends on the design of the luminosity monitor which increases the effectiveness of the mask. A significant part of these photons is produced by the electrons and positrons which do not enter the mask but are rather trapped outside of it. The number of these particles is about 37 per bunch crossing for TESLA and most of them hit the mask on the outside producing secondary photons.

A number of particles is produced at larger angles and transverse momenta. These can hit especially the vertex detector. Figure 2.4.11 shows the number of charged particles hitting the inner layer of the vertex detector. The radius of this layer is varied but the angular coverage of $|\cos\theta| < 0.98$ is kept constant. Below a radius of about 10 mm the number of hits increase drastically. In this case, the detector would be hit by particles that received their angles and transverse momentum by the deflection of the beams.

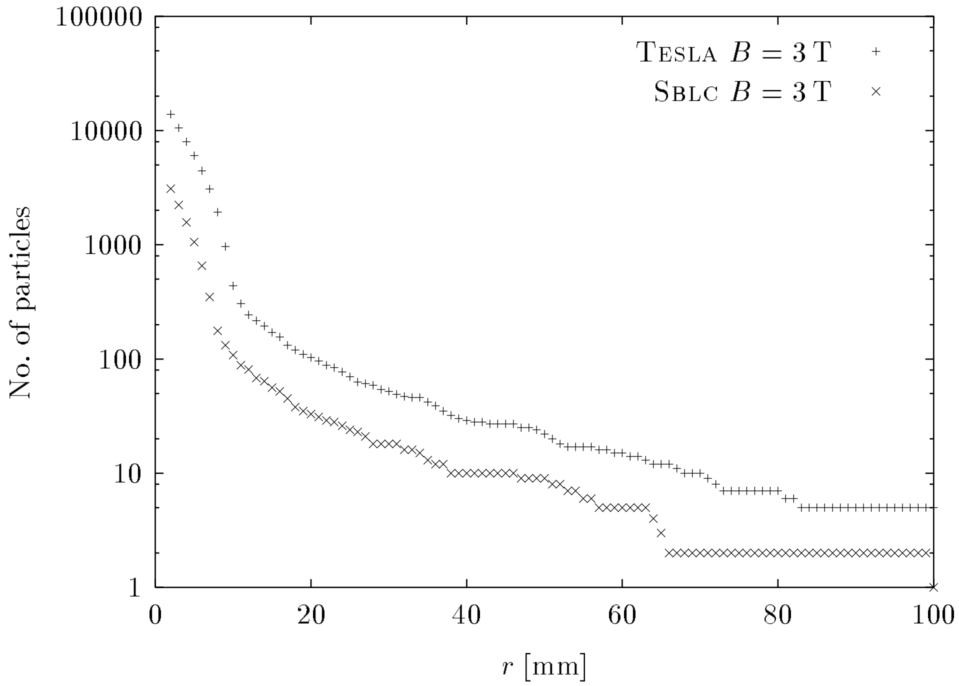

Figure 2.4.11: *The number of particles hitting the inner layer of the vertex detector as a function of its radius for an angular coverage of* $|\cos\theta| < 0.98$ *(for the* 500 GeV *c.m. parameters).*

The longitudinal and azimuthal distribution of the hits in the vertex detector layers is almost uniform with the center of the barrel showing a slightly higher hit density than the ends, see Fig. 2.4.12.

Almost all particles due to pair creation are lost inside the quadrupoles where the strong magnetic field bends their trajectories. At the ends of the quadrupoles facing the interaction point, the combined magnetic field of the outer main solenoid and quadrupole points towards the aperture. Soft charged particles produced in this region that leave the material of the quadrupole are led by these field lines back into the interaction point. The detector simulation shows that this can increase the number of hits in the vertex detector by an order of magnitude.

To suppress the backscattered charged particles an additional mask is used inside the main one. It consists of a material with a long radiation length (graphite) towards the interaction point to avoid particles scattering back at the mask. The other side is made of tungsten to reduce the background from the neutrons produced in the beamstrahlung collimator. The inner radius of the additional mask is set by the collimation system. The collimation is chosen such that no particle of the remaining tails could emit a photon in the final doublet that can hit the final doublet on the opposite side.

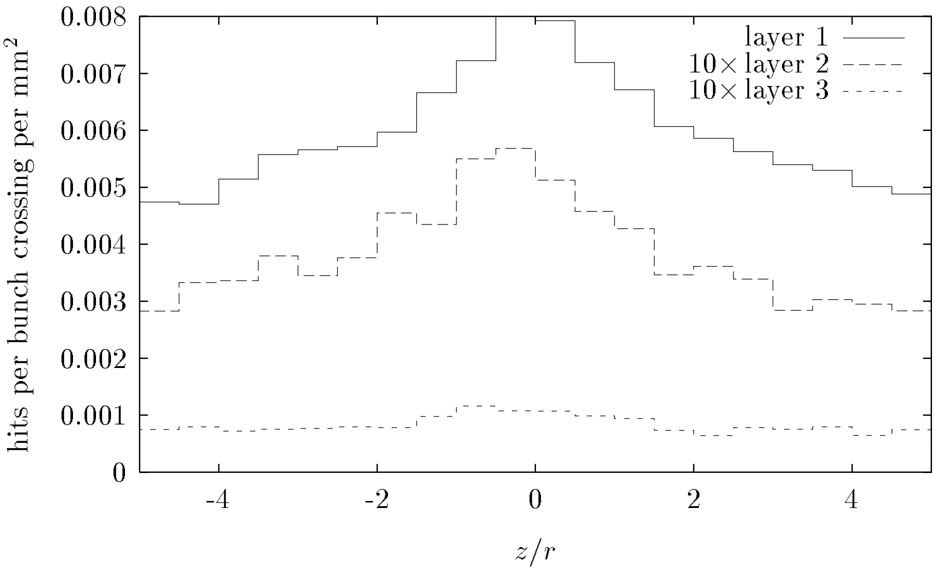

Figure 2.4.12: *The longitudinal distribution of the hits in the vertex detector for TESLA (*500 GeV *c.m.). The numbers for the layers two and three are enhanced by a factor ten. The azimuthal distribution is flat.*

In order to avoid that the additional mask can be hit by these photons its radius has to be at least 18 mm with the present collimation system (see Fig. 2.4.3). The radius of the beam pipe at the IP has to exceed the radius of the inner mask to achieve the suppression. It should therefore be at least 20 mm which leads to a minimal radius of the vertex detector of about 25 mm.

If it turns out to be desirable from the physics point of view to further reduce the beam-pipe radius at the interaction point in order to allow for a smaller radius for the vertex detector, this could be achieved by improving the collimation section and reducing the radius of the mask.

To avoid that the beam pipe is hit by a large number of particles which can emit bremsstrahlung photons its radius increases from 20 mm at $|z| = 125$ mm to 40 mm at $|z| = 750$ mm. In the simulation the inner most part of the beam pipe consists of a 1 mm thick beryllium tube while the outer parts are 1.5 mm thick. The detector simulation shows that the described mask suppresses the backscattering of charged particles to a negligible level.

At the radius of the vertex detector of 25 mm with an angular coverage of $|\cos\theta| < 0.98$ one finds about 230 hits per bunch crossing for TESLA which, including a safety factor of 1.5, leads to a hit density of about 10^{-2} mm^{-2}. For SBLC, the number of hits per bunch is 70, which leads to 1 hit per mm^2 and per bunch train.

As indicated in Fig. 2.4.10, low angle taggers will be incorporated inside the mask.

These could consist of tungsten calorimeters similar to those that are used presently for luminosity measurements. For TESLA, the simulation shows that the showers from the pair particles lead to soft photons with a total energy of about 250 GeV per side and bunch crossing in such low angle taggers. A single pair particle with an energy of more than 20 GeV would hit the tagger directly once per about 600 bunch crossings.

Photons in the electro-magnetic showers can produce neutrons via the giant resonance process. These neutrons have typical energies of around 1 MeV. For initial electrons with an energy of more than about 100 MeV the neutron yield is almost linear with the particle energy. In copper one neutron is produced per about 6 GeV, in tungsten per 2.5 GeV. The particles from pair production and bremsstrahlung produce about $6{\cdot}10^4$ neutrons per bunch crossing. In hydrogen rich material as for example scintillator low energy neutrons can produce slow protons which deposit their energy in a small distance via ionization.

An additional source of background is the production of hadrons by two colliding photons $\gamma\gamma \to \mathrm{X}$. In this process the photons fluctuate into hadrons with the same quantum numbers (usually ρ-mesons) and interact hadronically. The cross section for this process can be approximated as [13]

$$\sigma_H = 211\,\mathrm{nb} \cdot \left(\frac{s}{\mathrm{GeV}^2}\right)^{0.0808} + 297\,\mathrm{nb} \cdot \left(\frac{s}{\mathrm{GeV}^2}\right)^{-0.4525} \tag{2.4.1}$$

The hadronic content of the photon is suppressed if it has a significant virtuality. In the simulation this is taken into account by allowing for a maximal $Q^2 \leq 1\,\mathrm{GeV}^2$. For TESLA, the number of hadronic events with a center of mass energy in excess of 5 GeV is about 0.13 per bunch crossing. An event deposits on average an energy of 10 GeV at angles larger than 100 mrad in the detector.

Some of the hadronic events contain so-called minijets. These low energy jets can be produced via the direct process $\gamma\gamma \to \mathrm{q\bar{q}}$. Photons that interact as hadrons can also produce minijets if individual partons scatter either on the other photon (once-resolved process) or another parton from the other photon, which also interacts as a hadron (twice-resolved process), producing two minijets. The remnant part of the hadrons also forms jets with a small transverse momentum, the so-called spectator jets. While the cross section for the direct process decreases for higher photon-photon center of mass energies it increases for the once- and twice-resolved process, they can exceed the total hadronic cross section according to equation 2.4.1. This is not in contradiction if one assumes that at high center of mass energies the number of minijets per event increases rather than the number of events.

The simulation is performed using the parametrization of the partonic contents of the photon according to M. Drees and K. Grassie [14] as well as with the photon parametrization according to M. Glück, E. Reya and A. Vogt [15], which are compatible with measurements at HERA [16]. In TESLA the expected rate of minijets with a transverse momentum of 2.0 (3.2, 10) GeV/c is $(0.3, 0.0075) \cdot 10^{-2}$ per bunch crossing using the latter parametrization and thus significantly smaller than the total rate of hadronic events.

An additional background source are the beamstrahlung collimators which are located at a distance of about 120 m from the interaction point. These collimators are hit by around 200 kW of beamstrahlung photons, which produce about $8 \cdot 10^{13}$ neutrons per second adding both sides. Assuming a point-like source the neutron flux at the detector position is about $4.4 \cdot 10^4\,\mathrm{cm^{-2}s^{-1}}$ or about $4.4 \cdot 10^{11}\,\mathrm{cm^{-2}}$ per year. The detector can be shielded from these neutrons by a concrete wall but this has to have an inner hole to let the beams and the beamstrahlung photons pass. The effect of the inner mask on the neutron flux has been calculated using a simulation based on the GEANT/MICAP-interface and results in a suppression by three orders of magnitude for neutrons with an energy of less than about 100 MeV. Thus, the neutron flux is several orders of magnitudes lower than expected in the inner vertex detector layer of the proposed ATLAS experiment at LHC [17], which is around $6 \cdot 10^{13}\,\mathrm{cm^{-2}}$ neutrons per year.

The tungsten of the inner mask can be instrumented to measure the total energy deposition of the pair particles, which is about 9000 GeV per side and bunch crossing. This signal can be helpful for tuning the machine to achieve higher luminosity.

2.4.5 Ground Motion Detection and Feedback

Fast beam steering at the interaction point, which relies on the beam-beam effect of colliding bunches, is a powerful tool to relax nanometer tolerances for final focus quadrupoles in linear colliders. These tolerances are determined by the vertical spot size which is 16 to 19 nm in the case of SBLC or TESLA. One stringent requirement for such a feedback, which corrects the bunch train offset in the IP is, that the beam pulse is long compared to the overall processing time of the detected signal from the beam position measurement (BPM) to the kicker magnet. Due to the low frequency approach and especially in case of a superconducting linac this is naturally fulfilled.

Parameters that influence this delay are the distance of the beam position monitor to the IP, the processing time of the feedback loop and the required magnetic field strength compared to the available peak power of the amplifier. The amplitude of pulse to pulse ground motion which can be expected from measurements done in the HERA tunnel, which is a tunnel under the city of Hamburg with an colliding beam facility, [18, 19] is approximately 70 nm rms for frequencies above 1 Hz which is roughly 5 times the design vertical beam size. In order to limit the luminosity reduction to 5 %, the jitter at the IP should be smaller than 30 % of the beam size, which is roughly 5 nm in our case. A list of the interaction region parameters can be found in the machine chapter of this report. Additional measurements in an existing experimental hall in HERA (Hall West) over a typical distance of a linear collider final doublet of 4 to 6 m have been done. The correlation decreases significantly at frequencies higher than

10 Hz but integrated from here, the measured rms amplitudes are at least an order of magnitude smaller. Therefore the IP jitter during collision driven by uncorrelated motion of quadrupoles is expected to be much smaller than 70 nm.

One possibility to achieve this tolerance is to design a passive support system that keeps the final doublets at a given position over a time scale much larger than the repetition rate of the accelerator. This is certainly a challenging task for the technical design of the quadrupole supports which are part of the experiment in a linear collider. Independent of other methods for feedback, this design task should be fulfilled as good as possible to avoid additional complications like, for example, resonances induced by the support structure itself.

For a round beam the beam-beam force of two colliding bunches is proportional to the separation of the two bunches over approximately one sigma. Operating with an aspect ratio ($=\sigma_x/\sigma_y$) of 20 (or more) as it is foreseen in linear colliders to reduce the beamstrahlung, produces an almost linear beam-beam force over approximately $10\,\sigma_y$. According to the beam-beam simulations the kick angle per σ_y separation of the two colliding beams is given by approximately 30 to 60 μrad which can easily be measured with a BPM 2 to 3 m downstreams. At this position the beam offset in the monitor would be 100 μm per σ_y separation at the IP, which is easy to measure as compared to the 4 μm resolution being required for the rest of the linac BPMs.

A method based on beam-beam deflections to measure precisely the offset of the two colliding beams has been used for single bunch operation in the SLC from pulse to pulse already [20]. While at TESLA a bunch to bunch measurement of the beam position can be used for both outgoing beams within one pulse, in case of the SBLC, a combination of both methods is proposed which uses a pilot bunch in one of the two colliding beam pulses and only a single BPM in combination with a single kicker magnet [21]. A much more detailed discussion on the SBLC and TESLA feedback systems which are foreseen in the interaction regions can be found in this report in the sections where instrumentation and diagnostics are discussed.

2.4.6 Beam Related Measurements

2.4.6.1 Fast Luminosity Measurement

The normal operation of the collider requires on-line measurement of the luminosity in order to rapidly detect beam detuning at the IP. A fast re-tuning of the beam beam delivery system (BDS), by means of horizontal spot size and luminosity optimization, will also be integrated in the machine control. A relative luminosity measurement, eventually cross-calibrated with a slower but absolute measurement of large angle Bhabha pairs in the central detector, should be able to resolve luminosity variations of the order of 1% ideally within one bunch train: this would require a counting rate of about 10 events per bunch crossing for TESLA.

Low-angle Bhabha pairs emitted along the beam pipe, unless detected inside of the last quadrupole doublet, cannot be measured against the 200 kW of beamstrahlung photons emitted in a forward cone of about 1 mrad. This is why the fast luminosity monitor, like at the SLC [22], is based on the detection of the radiative Bhabha electrons and positrons. As shown by Fig. 2.4.8, in order to provide a clear signal, the energy of these particles, produced in the forward direction relative to the same-sign incoming beam, should range from about 20 GeV, above the pair-created background, to 100 GeV where the beamstrahlung spectrum starts to dominate.

As a result of a simulation taking into account the action of the opposite beam coherent electro-magnetic field as well as the weaker effect of the main solenoid on the emitted radiative Bhabha particles, Fig. 2.4.13 shows the rates of lost particles within

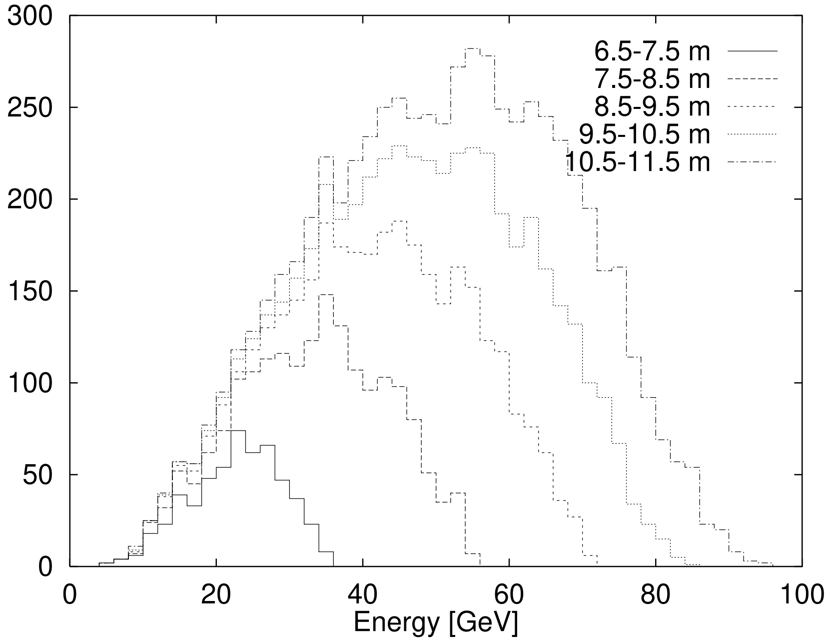

Figure 2.4.13: *Counting rates for radiative Bhabha electrons and positrons lost in the given z-ranges per bunch crossing for TESLA (*500 GeV *c.m.)*

different 1 m longitudinal ranges after the last doublet exit. Due to the peculiarities of the beam-beam and quadrupole focusing forces, all of these particles are lost in the horizontal plane. Located between 8.5 and 9.5 m, a luminosity detector would intercept particles around 50 GeV in energy and would be free from the background of outgoing beam particles with energies higher than 80 GeV, lost downstream.

The present ALEPH-BCAL calorimeter [23], designed to detect 45 GeV horizontal Bhabha pairs at LEP, would therefore be a good prototype for such a detector. Al-

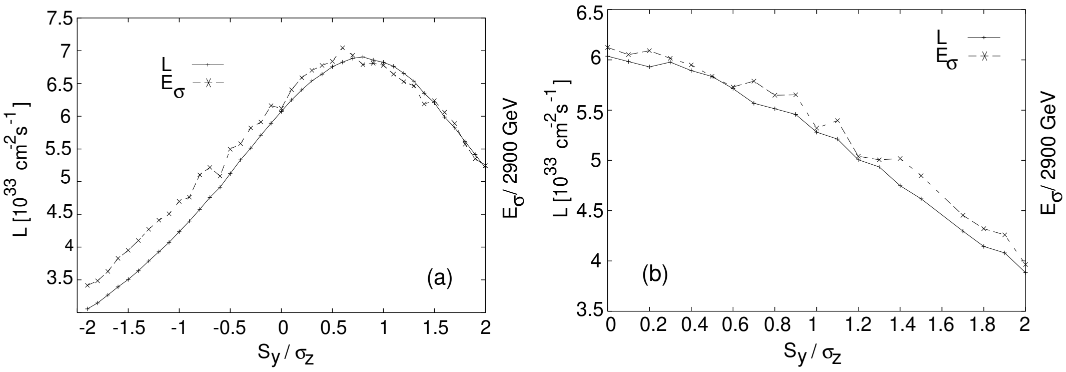

Figure 2.4.14: *Comparison of luminosity* L *and energy* E_σ *deposited by the* e^+e^- *pairs in the inner part of the mask if (a) the two vertical waists are symmetrically shifted by* S_y *with respect to the collision point along the beam axis and (b) for two coinciding vertical waists which are shifted with respect to the collision point, for TESLA (*500 GeV *c.m.) parameters.*

though its insertion and actual acceptance has not been calculated precisely, the total rate of about 5500 electrons and positrons lost in the 8.5 to 9.5 m range with an energy higher than 30 GeV suggests that the 1 % relative accuracy may be a realistic goal.

By instrumenting the inner part of the mask as a calorimeter one can use the total energy deposited by the pairs in this region to optimize luminosity. The signal depends on the produced photon spectrum, the luminosity and the deflection of the pairs by the beams. For constant bunch length, width and charge the spectrum and deflection are almost constant with a very weak dependence on the vertical bunch size. The deposited energy then depends only on the number of produced pairs which is proportional to luminosity.

One reason for a decreased luminosity is a shift of the vertical waists of the beams. In this case the position where the beam reaches its smallest vertical size lies either before ($S_y > 0$) or behind ($S_y < 0$) the collision point. Figure 2.4.14(a) shows the dependence of the luminosity and the pair energy deposited in the inner mask for two symmetrically shifted vertical waists. Optimal luminosity is reached if both beams are focused slightly before the collision point. Figure 2.4.14(b) shows the dependence of the luminosity and energy deposition if the two waists are at the same position but are shifted with respect to the collision point.

The achievable resolution has to be studied in detail. The main error may be due to changing bunch properties like the horizontal and longitudinal dimensions. With knobs to tune the vertical waist shift only, the relative signal can be used to maximize luminosity.

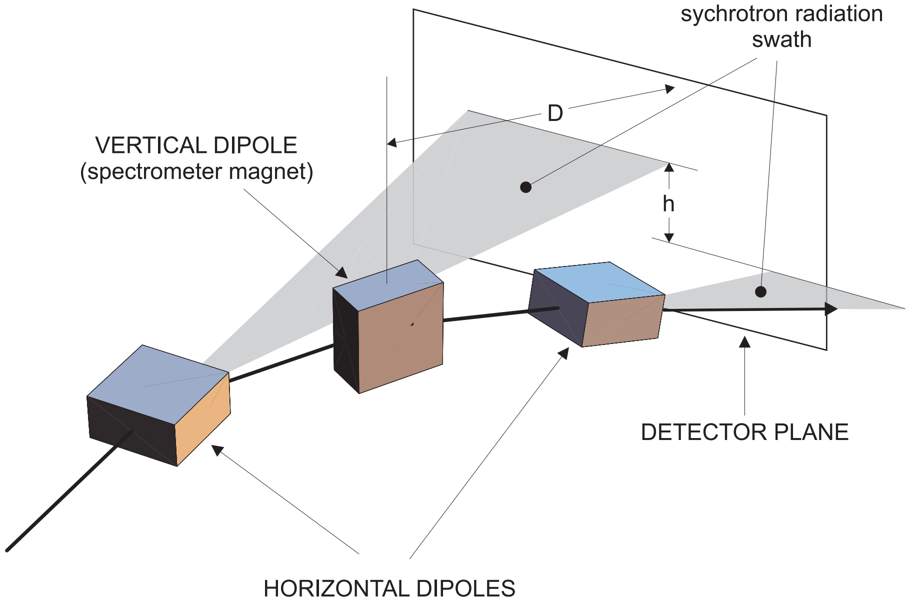

Figure 2.4.15: *Energy Spectrometer Concept (as used at the SLC/SLD). The vertical bend acts as the spectrometer magnet, while the two horizontal dipoles produce swaths of synchrotron light which are detected a distance D downstream. The bend angle (and hence the momentum) of the beam is given by h/D [not to scale].*

2.4.6.2 Energy Measurement

It is intended to place two precision spectrometers in both the electron and positron extraction lines to order to determine the absolute energy of each beam with a resolution of 10^{-4}. Since the beams are expected to loose some 3 % of their energy during the beam-beam interaction, it will be necessary to turn one beam off in order to make a measurement of the pre-collision energy of the other beam. Spectrometers based on the same design currently used at the SLC with a $5{\cdot}10^{-4}$ resolution will be used [24], a schematic of which is shown in Fig. 2.4.15. The spectrometer consists of a single high precision spectrometer magnet, either side of which are two small synchrotron light generating dipoles whose deflecting angles are in the opposite plane to the spectrometer magnet. The separation of the two bands of synchrotron light generated is measured by a suitable synchrotron radiation detector placed an accurately known distance downstream from the spectrometer magnet. The separation is proportional to the bend angle of the spectrometer magnet and hence the energy of the beam. At 250 GeV, a spectrometer magnet of length 5 m and field 0.24 T generates a bend angle of approximately 1.5 mrad. The energy loss from the magnet is approximately 25 MeV or 0.01 % which is acceptable given the required resolution.

Another method for measuring the absolute center of mass energy, based on radiative Z boson production and the precise knowledge on the Z mass, is described in section 2.3.1.2 of this chapter.

2.4.6.3 Polarization Measurement

The longitudinal polarization of the electron beam, expected to be about 80 %, can be measured with a Compton polarimeter similar to the ones already used at SLAC [25] and DESY [26]. The longitudinal polarization P_e of the electron beam is extracted from the asymmetry between 2 measurements of Compton scattering with parallel (+) or anti parallel (−) polarization of the electron and Laser beams. Kinematics and cross-sections of Compton scattering of 250 GeV electrons on 2.33 eV photons, corresponding to a green ($\lambda = 532$ nm) Nd:YAG laser, are shown in Figs. 2.4.16 and 2.4.17 from Ref. [27] where 1064 nm IR and 248 nm UV lasers have also been studied. As can be seen, the asymmetry is maximum when the photons are recoiling along the electron axis with the maximum energy of 225 GeV.

The time t needed to measure the electron polarization to an accuracy $\Delta P_e/P_e$ is given by

$$t = \frac{1}{\mathcal{L}\ \left(\frac{\Delta P_e}{P_e}\right)^2\ P_e^2 P_\gamma^2}\ \frac{1}{A^2}\ \frac{1}{\sigma(k'_{\gamma,\mathrm{min}})} \tag{2.4.2}$$

where $\mathcal{L}$ is the luminosity, A is the measured asymmetry and $\sigma(k'_{\gamma,\mathrm{min}})$ the total cross-section above a photon energy detection threshold $k'_{\gamma,\mathrm{min}}$. For TESLA, assuming a electron beam spot size of 20 μm, a 1 W cw laser and a 10 mrad electron-laser crossing angle, the luminosity has been estimated to be about $5 \cdot 10^{26}\,\mathrm{cm}^{-2}\mathrm{s}^{-1}$. For a completely polarized laser $P_\gamma = 1$, the time needed for a 1 % accurate polarization measurement is then of the order of 15 min. This time could be considerably reduced by using a pulsed laser with a higher peak power synchronized with the electron bunch train. In this case, one could even pulse the laser every few bunch trains for a precise determination of the background.

The insertion of the Compton polarimeter has not been studied yet. Locating the Compton interaction point after the e^+e^- collision point would allow to measure the polarization of the electron beam with and without collisions in such a way that the depolarization due to the beam-beam forces, predicted to be negligible, could be detected. Locating it in front of the separator would allow to analyze the recoiling electron momentum in the separator deflecting field, as is done at SLAC [25], rather than the very high energy photon scattered in the forward direction. Locating the polarimeter downstream the extraction line would require a precise knowledge of the spin transport optics as well as that of the electron beam transverse polarization to reconstruct the longitudinal polarization at the IP.

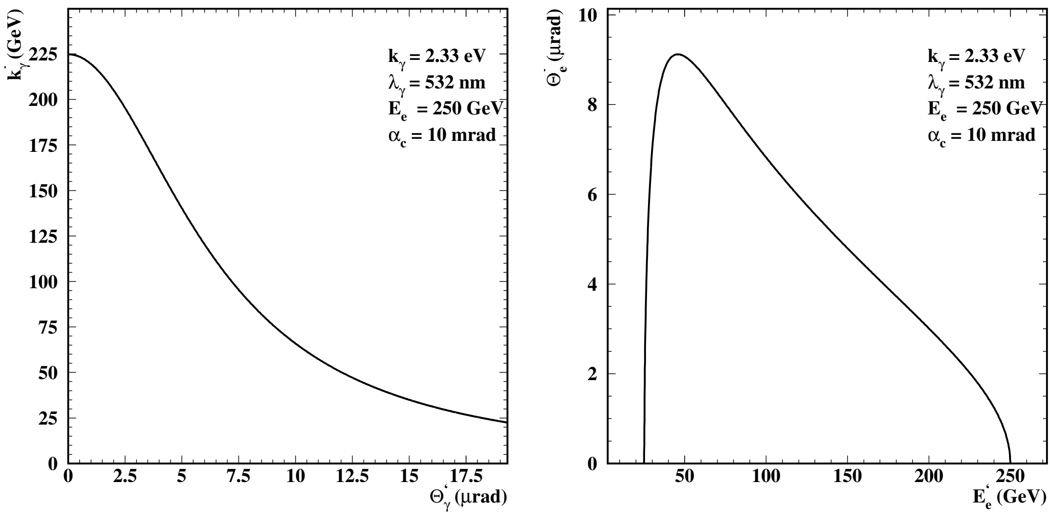

Figure 2.4.16: *Kinematic of the Compton scattering. Scattered γ energy k'_γ as a function of scattered γ angle θ_γ (left). Scattered* e^- *energy E'_e as a function of scattered* e^- *angle θ_e (right).*

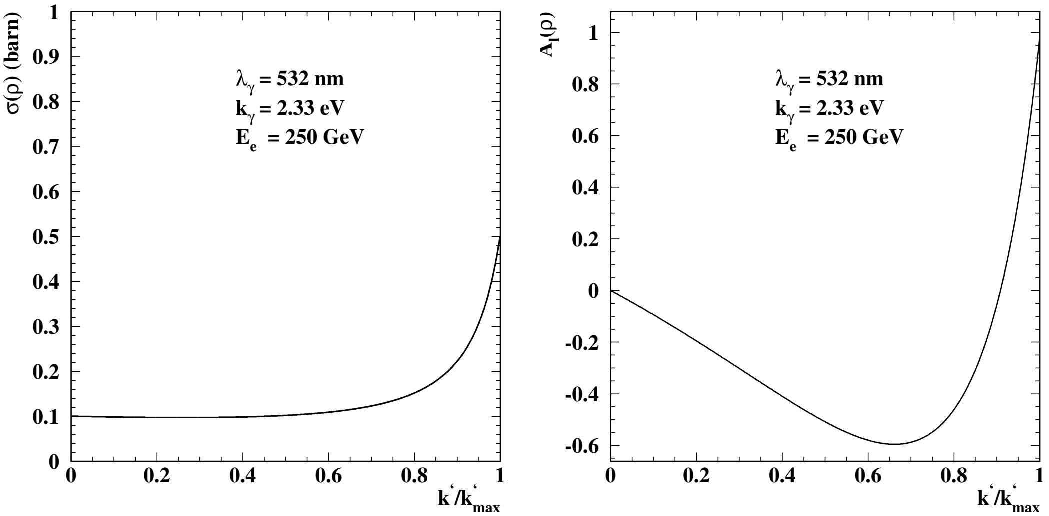

Figure 2.4.17: *Compton unpolarized differential cross section and longitudinal asymmetry as a function of the scattered photon energy k'_γ.*

2.4.6.4 Beam Size Measurement

The beam sizes to be measured at the interaction point (IP) are extremely small: less than 20 nm vertical and less than 1 μm horizontal. The precision should be better than 10 %. Beam sizes as small as 70 nm have already been measured at the Final Focus Test Beam (FFTB) at SLAC [28] with a Shintake-Monitor [29]. At SLD, a laser wire is used to measure beam sizes down to 1 μm [30]. It is planned to use both techniques at the IP: the Shintake-Monitor for the vertical beam size and the laser wire for the horizontal beam size.

Shintake-Monitor The Shintake-Monitor uses the two arms of a split laser beam to generate an interference pattern at the location of the electron beam. The spacing between the fringes is a few times larger than the beam size to be measured. The electron beam is swept over the pattern using a steering magnet. The rate of Compton scattered photons N_γ is measured as a function of the beam displacement y. The result is a modulated signal, where the modulation depth is a direct measure of the beam size. Figure 2.4.18 shows the principle components of the system.

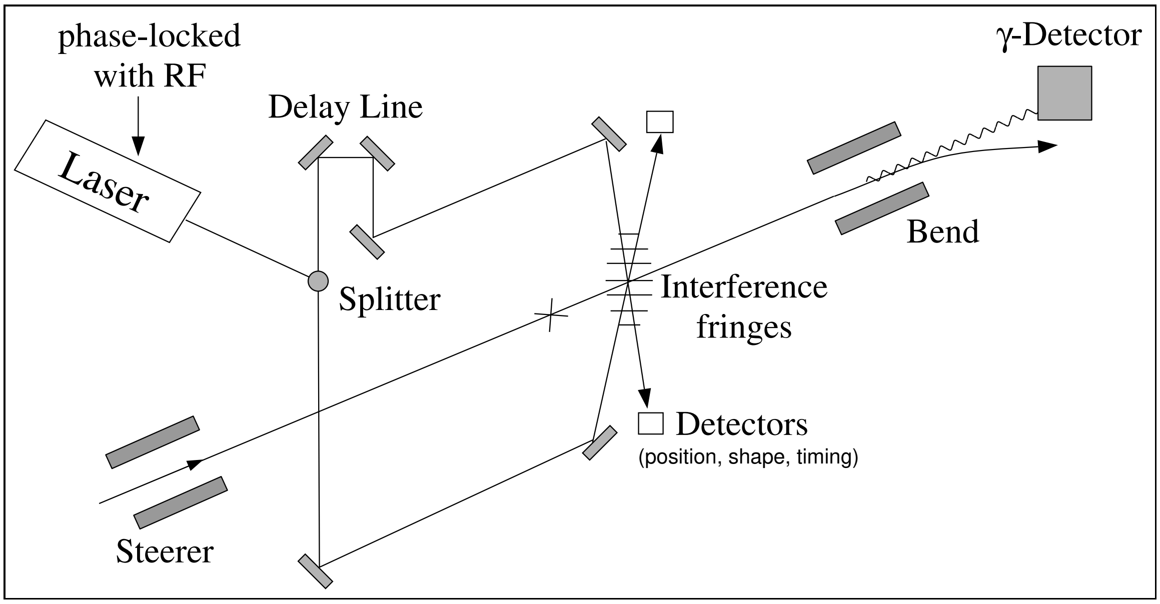

Figure 2.4.18: *Shown are the principal components of the Shintake-Monitor at the interaction point. The electron or positron beam is swept over the fringe pattern generated by the two arms of the split laser beam. The Compton scattered photons are measured as a function of the sweep.*

The advantage of this technique is the precise knowledge of the fringe pattern. The distance d between the fringes is only a function of the laser wavelength λ, if the angle θ between the laser arms is chosen to be close to 180°: $d = \lambda/(2\sin(\theta/2))$. A quite large misalignment in the angle of 1° would result in an uncertainty of the beam size of only 1 %.

The measured modulated Compton rate $N_\gamma(y)$ is fitted to a sine-function in order to determine the modulation depth $M = (N_{\rm max} - N_{\rm min})/(N_{\rm max} + N_{\rm min})$ (see Fig. 2.4.19a). The modulation depth is a function of the beam size σ [29]:

$$M(\sigma) = K|\cos\theta| \mathrm{e}^{-2(\frac{2\pi}{\lambda}\sin\frac{\theta}{2})^2\sigma^2}$$

For realistic assumptions, the correction factor K is 0.996 for TESLA and 0.994 for SBLC. It accounts for a power imbalance of the two laser beam arms of 10 % and the finite laser beam spot size in z of $w = 10\,\mu$m. The latter correction is small and depends only weakly on σ, since the laser beam waist w is small compared to the beta-function of the electron beam ($\beta_y^\star = 700\,\mu$m for TESLA and $450\,\mu$m for SBLC). In order to keep the traveling wave component small, θ should be close to 180°. For practical reasons and the necessity to monitor the outgoing laser beams, $\theta = 175°$ is chosen.

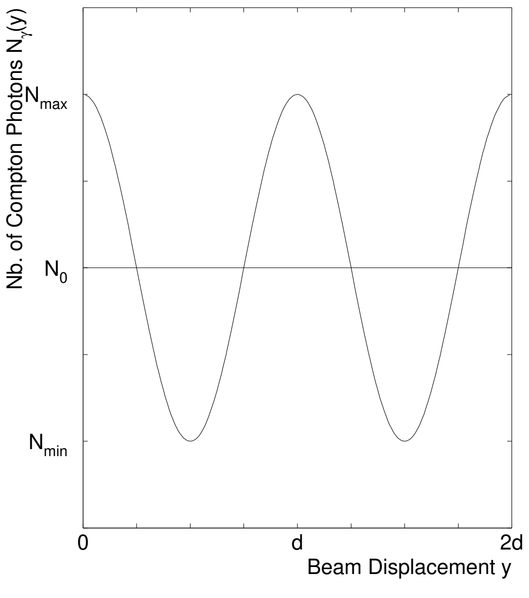

(a)

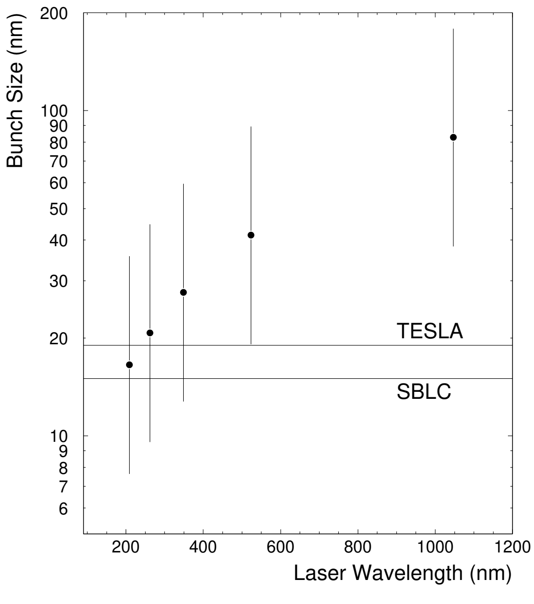

(b)

Figure 2.4.19: *(a) Modulated signal* N_γ *as a function of the beam displacement* y*;* d *is the fringe distance. (b) The lines indicate accessible beam size ranges for the different wavelengths of a Nd:YLF laser. The black dots are for a modulation depth* M *of* 0.61 *(best sensitivity), the range indicated is for* M *between* 0.1 *and* 0.9 *(*$\theta = 180°$*).*

The best sensitivity for a given beam size is achieved, when the laser wavelength is chosen such, that the modulation depth M depends strongest on the beam size: $\mathrm{d}M/\mathrm{d}\sigma$ is maximal when $\lambda = 4\pi\sigma\sin(\theta/2)$. In the following, $\theta = 180°$ is assumed. The optimal wavelengths for bunch sizes of 16 and 19 nm are 201 and 239 nm resp. Common lasers for these wavelengths are Excimer lasers (ArF 193 nm, KrF 248 nm) and higher harmonics of Nd doped lasers like Nd:YLF (209 nm and 262 nm).

The expected measurement error depends mainly on the signal-to-noise ratio of the measured Compton photons. Other sources contributing to the systematic error are the position jitter and injection angle of the electron beam, and a misalignment and a non-uniformity of the laser beam. At the FFTB, these parameters have been controlled in a way that the beam size measurement error was about 7 % [28]. The electron position jitter has to be much smaller than the bunch size to be measured. It is expected that for TESLA and SBLC this is the case at least during one bunch train.

The dynamic range of the Shintake-Monitor is small: taking the measurement error of the modulation depth from the FFTB of $\mathrm{d}M = 0.02$, the relative error in the beam size is less than 10 % for a modulation depth M in the range of 0.1 and 0.9. Using e.g. a laser wavelength of 262 nm, beam sizes between 10 and 45 nm can be measured within this range. Figure 2.4.19b shows the accessible beam size ranges for some harmonics of a Nd:YLF laser. A laser based on Nd:YLF[4] would cover the beam sizes from 8 to 180 nm. Therefore, it is planned to use at least the fundamental, the second and fourth harmonic in order to be able to measure larger than nominal beam sizes as well. To extend the range to 1 μm, a CO_2 laser ($\lambda = 10\,\mu$m) may be used, or the angle θ between the laser arms may be reduced e.g. to the cone opening angle of 200 mrad.

The expected mean number of Compton scattered photons per bunch N_γ can be estimated from

$$N_\gamma = \sigma_c N_e n_{\mathrm{ph}} L$$

The Compton cross section is $\sigma_c = 1.7{\cdot}10^{-24}\,\mathrm{cm}^2$ for a beam energy of 250 GeV and a laser wavelength of 262 nm. The product of the laser photon density and the target length $n_{\mathrm{ph}}L$ can be expressed by $n_{\mathrm{ph}}L = \sqrt{\frac{2}{\pi}}\frac{P}{c^2 h}\frac{\lambda}{w}$ assuming gaussian distributions for the laser beam. P is the power of the laser, w the laser beam waist. With $\lambda = 262$ nm and $w = 10\,\mu$m we get

$$N_\gamma = 600 \cdot N_e/(10^{10}) \cdot P/(MW)$$

To achieve approximately the same photon yield per bunch as the FFTB, 0.2 MW of laser power are required. The correction due to the gaussian shape of the electron beam reduces the rate by 15 %.

For the photo injector of the Tesla Test Facility (TTF) a laser is being built [31], which fulfills most of these requirements. This laser will deliver a train of more than

[4] Lasers based on materials doped with Nd like Nd:YAG, Nd:YLF or Nd:Glass have all similar wavelengths.

800 pulses spaced by 1 μs with a repetition rate of 10 Hz. The pulse length is about 10 ps. It is straightforward to modify this laser to reflect the TESLA bunch structure. To generate the SBLC bunch structure would not impose principle problems, only the laser power per pulse must be at least doubled, since the 5^{th} harmonic is preferred for a bunch size of 16 nm. Table 2.4.2 shows the numbers of expected Compton scattered photons for a TTF type laser system.

The laser pulses are synchronized with the electron bunches, and will allow a bunch-to-bunch measurement. Within a bunch train, a full sweep over the interference pattern will be measured. The laser pulse repetition rate in the train should be half the electron bunch rate allowing the determination of the background every second bunch.

λ (nm)	P (MW)	N_γ (TESLA)	N_γ (SBLC)
1047	15	25500	7730
523.5	7.5	14450	4380
262	3	6440	1950
209	1	2200	670

Table 2.4.2: *Shown are the expected number of Compton scattered photons N_γ per bunch for a TTF-type laser system. The laser is focused to a waist of $w = 10\,\mu$m. The laser power P for the different wavelengths λ are the expected performances of the TTF laser.*

Since the laser pulses are short (in the order of 10 ps), the requirements on the timing and alignment of the laser beams are tight. The path length difference of the two arms has to be smaller than 1 mm. A remotely controlled delay line, motorized mirrors, and suitable fast detectors are required to adjust and stabilize the beams.

For stability reasons, the last optical elements, the mirror and focusing optics will be mounted onto the detector mask, which itself is a heavy rigid structure. Incorporating most of the optics into the mask reduces additional dead material inside the detector to a minimum. The laser will be housed outside the detector. The split laser beams of the different wavelengths will be transported into the detector with a mirror system [32]. The system will be installed on both sides of the detector. The mask will not extend to the interaction point. Therefore, the electron or positron beam focus has to be shifted from the IP about 800 mm up- and downstreams.

Special attention has to be taken on the laser beam intensity at the mirror surfaces: the peak intensity on the last mirror is about 100 MW/cm^2 per MW laser beam power in one arm. For several MW of laser power, the intensity comes close to damage thresholds of common dielectric mirrors, which are in the order of 1 GW/cm^2. Therefore, critical parts of the laser beam line should be evacuated to a pressure of less than 10^{-6} mbar to avoid dust particles on the mirror surfaces. Therefore, it is planned to include the last critical mirrors for the Shintake Monitor as well as for the laser wire into the vacuum of the beam pipe (see Fig. 2.4.20).

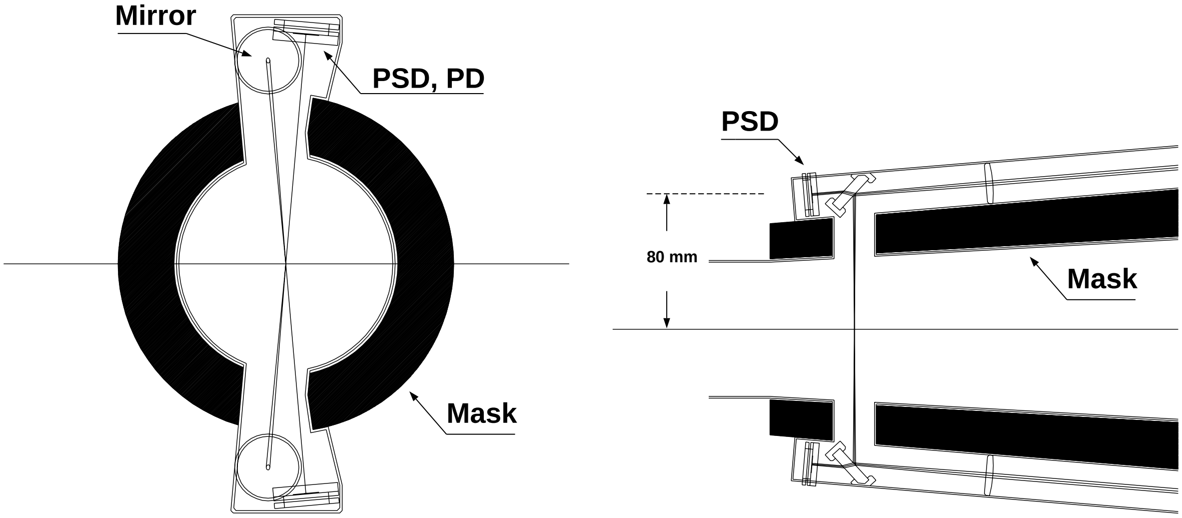

Figure 2.4.20: *Possible mechanical implementation of the optics for the Shintake Monitor. On the left, the $r\phi$-view is shown, indicating a position sensitive device (PSD) and a fast diode (PD) for timing. The z-view on the right shows how the beam is guided along the mask.*

Laser Wire The laser beam is used in a similar way as a wire in wire scanners. The beam is swept over a strongly focused laser beam. From the measured rate of Compton-scattered photon N_γ as a function of the beam displacement y, the size of the beam can be determined by unfolding the signal with the shape of the laser beam. In order to reduce potential systematic errors due to the uncertainties in the laser beam shape, the laser spot should be smaller than the beam size. Assuming a perfect gaussian transverse laser beam (TEM$_{00}$-mode), the waist $w = 2\sigma_r$ at the focal spot is given by $w = \lambda/\pi\theta$, where θ is the far field divergence angle of the laser beam with a wavelength λ. To estimate the achievable spot size, the geometrical constraints at the IP have to be considered. The last optical elements for the laser wire will be mounted onto the detector mask at a distance of about 1 m from the IP. At this location, the last focusing mirror will be at a distance from the electron beam line of about $l = 100\,\mathrm{mm}$. Allowing a laser spot diameter at the last mirror of $D = 30\,\mathrm{mm}$, the smallest achievable waist would be $w = \frac{\lambda}{\pi}/\arctan(\frac{D}{2l}) \approx 2\lambda$. Choosing the 4$^{\mathrm{th}}$ harmonic of a Nd:YLF laser (262 nm), a spot size down to 560 nm could be realized for perfect conditions.

This is smaller than the TESLA horizontal beam size of 845 nm, but still larger than the SBLC beam size of 335 nm. Either the smallest transmittable wavelength through air has to be chosen (ArF-Excimer with 193 nm) or the Shintake-technique may be used. However, for $\theta = 180°$, the optimal wavelength would be 4210 nm, where no common laser source exists. But reducing the angle between the two laser beams to $\theta = 29°$, a standard Nd-doped laser material could be used.

The number of scattered Compton photons N_γ can be estimated assuming gaussian shapes for the electron bunch as well as for the laser bunch: for a laser wavelength of 262 nm and a laser spot size of $w = 600$ nm one gets for TESLA, if both beams are centered,

$$N_\gamma = 3000 \cdot N_e/(10^{10}) \cdot P/(MW)$$

which is sufficient for a reasonable measurement.

Compton-Detector For the Shintake-Monitor and the laser wire the detector for the Compton scattered photons will be far behind the bend of the beam delivery system at a distance of about 100 m from the IP (see Fig. 2.4.1). Most of the scattered photons will have 70 to 90 % of the beam energy. Their angle with respect to the beam axis is proportional to $1/\gamma$ and in the order of $10\,\mu$rad. This is small enough to pass through the beam pipe and the collimators.

2.4.7 Luminosity expectation for a calibration run on the Z^0-pole

The aspects of running the TESLA collider on the Z^0-pole, corresponding to a center of mass energy of 91.2 GeV well below the design energy, have not been studied in any detail. The following considerations are therefore preliminary.

The main uncertainty in the luminosity of a dedicated run on the Z^0-pole comes from the positron intensity. The present design of the positron source relies on using the high energy electron beam, captured after the collision, as the primary beam for intense production of photons in a long wiggler. The photons are then converted into positrons on a target. This concept requires a primary beam energy above 150 GeV to produce the desired positron intensity. Below this energy, an auxiliary classical positron source is needed whose performance has not been fully analyzed yet.

However the luminosity obtainable in the Beam Delivery System (BDS) at 91.2 GeV as compared to 500 GeV c.m. energy can be analyzed, if one assumes 1) that the beam normalized transverse emittances are identical for both energies (this may require the use of bypass beam lines to extract both beams at 45.6 GeV from the linacs), 2) that the BDS magnet strengths can be powered down linearly with the energy in such a way that the Twiss parameters are essentially identical along the BDS, keeping the freedom to re-match the beta-functions at the IP with the quadrupoles of the beta matching section, 3) that the electron bunch train matches the positron one both in time structure and in beam size.

Then, the luminosity scales according to the following expression

$$\mathcal{L} \propto \frac{I^+ N^-}{\sigma_x^* \sigma_y^*} \times H_D$$

where I^+ is the positron current, N^- the electron bunch charge, σ_x^* and σ_y^* are the transverse beam sizes and H_D is the pinch enhancement factor.

The electron bunch charge N^-, which is $3.6{\cdot}10^{10}$ for the 500 GeV design, can probably be raised up to $5{\cdot}10^{10}$, as in a previous parameter list.

In view of the uncertainty in the positron bunch population, the pinch factor, which is equal to 1.65 in the 500 GeV design, must be assumed equal to unity.

The vertical beam size σ_y^* is fixed by the hour-glass condition $\beta_y^* = \sigma_z$, where σ_z is the bunch length. It therefore scales like the square-root of the energy up to $\sigma_y^* = 44.5\,\mathrm{nm}$. This implies that the beam divergence Θ_y^* at the IP, and hence the 1-sigma beam size in the last doublet, is also increased by the same factor. However, this has a detrimental impact neither on the Oide effect which scales like $(\Theta_y^* \cdot \gamma)^5$ and therefore gets weaker, nor on the synchrotron radiation background which is governed by the product $(N_y^{\mathrm{coll}} \cdot \Theta_y^*)$ where N_y^{coll} is the collimation condition in units of σ_y. Assuming that the vertical collimator gaps are identical for both energies, N_y^{coll} scales inversely with the square-root of the energy, and therefore the synchrotron radiation stay-clear is identical (with a reduction in the photon numbers and photon energies, strongly dependent on the beam energy).

The horizontal beam size is the only parameter which can be used to sizeably increase the luminosity on the Z^0-pole. The above discussion for the vertical beam size shows that it is safe to scale σ_x^* with the square-root of the energy up to $\sigma_x^* = 2\,\mu\mathrm{m}$. The constraint on the large aspect ratio from the beamstrahlung is of course relaxed at the low energy: even at the nominal bunch population of $3.6{\cdot}10^{10}$ for both beams, the beamstrahlung energy loss is of the order of 1 % for $\sigma_x^* = 1\,\mu\mathrm{m}$. Therefore, σ_x^* can be decreased as long as a higher level of synchrotron radiation background, or alternatively a higher level of muon background by tightening the horizontal collimators, can be accepted for the Z^0-pole running experiment.

The above discussion shows that the luminosity would simply scale linearly with the energy if the positron intensity $I^+(46.5\,\mathrm{GeV})$ at the Z-pole could be maintained at the same level as $I^+(250\,\mathrm{GeV})$ at 500 GeV c.m. energy. It would also benefit from a larger pinch enhancement factor due to the stronger pinch effect at low energy. For a reduced positron intensity, the above arguments suggest that the luminosity is given by

$$\mathcal{L} \simeq 9.1 \cdot 10^{32}\,\mathrm{cm}^{-2}\mathrm{s}^{-1} \cdot \frac{I^+(46.5\,\mathrm{GeV})}{I^+(250\,\mathrm{GeV})} \cdot \frac{2\,\mu\mathrm{m}}{\sigma_x^*}$$

The target value of $10^{32}\,\mathrm{cm}^{-2}\mathrm{s}^{-1}$ luminosity, which corresponds to about 11,000 Z^0 per hour, could therefore be achieved with a factor 10 (for $\sigma_x^* = 2\,\mu\mathrm{m}$) or 20 (for $\sigma_x^* = 1\,\mu\mathrm{m}$) reduction in the positron intensity. Intensity reduction factors of the order of 100 would lead to luminosities in the range of $10^{31}\,\mathrm{cm}^{-2}\mathrm{s}^{-1}$.

Bibliography

[1] O. Napoly, E. Klein and J.M. Rifflet, "TESLA Final Focus System with Superconducting Magnets in the Interaction Region", Saclay Preprint, DAPNIA/94-10 (1986).

[2] R. Jacobsen et al., "Detector background conditions at linear colliders", SLAC-PUB-5205 (April 1990).

[3] L.P. Keller, SLAC-PUB-5522 (April 1991);
L.P. Keller, SLAC-PUB-6385 (October 1993).

[4] CERN Program Library, GEANT 3.15, W5013.

[5] M. Sachwitz, H.J. Schreiber, "Muon Background in a 500 GeV TESLA Linear Collider", DESY Print, November 1994, TESLA 94-27.

[6] Yung-Su Tsai, Rev. Mod. Phys. 46 (1974) 815.

[7] E. Kushnirenko, in Proc. of the International Workshop on Final Focus and Interaction Regions of Next Generation Linear Colliders, SLAC-405, (1992).

[8] N.V. Mokhov, "Comparison of Backgrounds in Detectors for LHC, NLC and $\mu^+\mu^-$ Colliders", Fermilab-Conf-96/062 (1996).

[9] A.I. Drozhdin, M. Huhtinen and N.V. Mokhov, "Accelerator Related Background in the CMS Detector at LHC", Fermilab-Pub-96/113 and CERN-CMS-TN/96-056 (1996); to be published in Nucl. Instrum. and Meth.

[10] N.V. Mokhov, "The MARS Code System User's Guide", Version 13(95), Fermilab-FN-628 (1995).

[11] K. Yokoya and P. Chen, "Beam-beam phenomena in linear colliders", KEK Preprint 91-2 (1991).

[12] D. Schulte, "Study of Electromagnetic and Hadronic Background in the Interaction Region of TESLA", Ph.D. thesis, University of Hamburg 1996.

[13] T. Sjoestrand, "What is a photon and how should it diffract?", Talk given at Photon 95.

[14] M. Drees and K. Grassie, "Parametrizations of the photon structure and applications to supersymmetric particle production at Hera", Zeitschr. f. Phys. C, 28 (1985) 451–462.

[15] M. Glück, E. Reya, and A. Vogt, "Photonic parton distributions", Physical Review D, 46 (1992) 1973.

[16] J.M. Butterworth, "Photon Structure as seen at HERA", DESY 95-043, March 1995.

[17] ATLAS collaboration, "Technical proposal for a general-purpose experiment at the large hadron collider at CERN", CERN/LHCC/94-43 (1994).

[18] V. Shiltsev, B. Baklakov, P. Lebedev (Novosibirsk, IYF), C. Montag, J. Rossbach (DESY), "Measurements Of Ground Vibrations And Orbit Motion At HERA", DESY-HERA-95-06, June 1995, 64pp.

[19] R. Brinkmann, J. Rossbach (DESY), "Observation Of Closed Orbit Drift At Hera Covering Eight Decades Of Frequency", Nucl. Instrum. and Meth. A350 (1994) 8-12.

[20] P. Bambade, R. Erickson, "Beam-Beam Deflections as an Interaction Point Diagnostics for the SLC", SLAC-PUB-3979, May 1986.

[21] G.A. Voss, R. Brinkmann, N. Holtkamp. "A Beam Based Interaction Region Feedback for an SBLC Linear Collider", Linac 96, Linac Conference, Aug. 1996, CERN, Geneva, to be published.

[22] R.C. Field, private communication.

[23] E. Fernandez et al., "A very forward luminosity monitor for the ALEPH detector at LEP", Nucl. Instrum. and Meth. A297 (1990) 153.

[24] Mark II Collaboration and the SLC Final Focus Group, SLAC-SLC-PROP-2 (1986).

[25] G. Shapiro et al., "The Compton Polarimeter at the SLC", Proc. of the "1993 IEEE Particle Accelerator Conference", May 17-20, 1993, Washington DC, p. 2172.

[26] D.P. Barber et al., "The HERA polarimeter and the first observation of electron spin polarization at HERA", Nucl. Instrum. and Meth. A329 (1993) 79.

[27] G. Bardin, C. Cavata and J.P. Jorda, "Compton Polarimeter studies for TESLA", DESY Print, TESLA 97-03.

[28] V.A. Alexandrof et al., "Results of Final Focus Test Beam", Proc. of the "1995 IEEE Particle Accelerator Conference", May 1–5, 1995, Dallas (Texas), p. 2742.

[29] T. Shintake, "Proposal of a nanometer beam size monitor for e^+e^- linear colliders", Nucl. Instrum. and Meth. A311 (1992) 453.

[30] D. Arnett et al., "SLC/SLD Laserwire", Proc. of the "6th Intern. Workshop on Linear Colliders LC95", ed. J. Urakawa, March 27–31, 1995, Tsukuba, Japan, KEK proceedings 95-5, p. 1525.

[31] "Tesla Test Facility Linac – Design Report", Ed.: D.A. Edwards, DESY Print, March 1995, TESLA 95-01.

[32] see e.g.: O. Biebel et al., "The Laser System for Calibration and Monitoring of the OPAL Jet Chamber", Nucl. Instrum. and Meth. A320 (1992) 183.